
The Malignant Tail: Spectral Segregation of Label Noise in Over-Parameterized Networks

Zice Wang¹

Abstract

While implicit regularization facilitates benign overfitting in low-noise regimes, recent theoretical work predicts a sharp phase transition to harmful overfitting as the noise-to-signal ratio increases. We experimentally isolate the geometric mechanism of this transition: the **Malignant Tail**, a failure mode where networks **functionally segregate** signal and noise, reducing coherent semantic features into low-rank subspaces while pushing stochastic label noise into high-frequency orthogonal components, distinct from systematic or corruption-aligned noise. Through a Spectral Linear Probe of training dynamics, we demonstrate that Stochastic Gradient Descent (SGD) fails to suppress this noise, instead **implicitly biasing** it toward high-frequency orthogonal subspaces, effectively preserving signal-noise separability. We show that this geometric separation is distinct from simple variance reduction in untrained models. In trained networks, SGD actively segregates noise, allowing post-hoc Explicit Spectral Truncation ($d \ll D$) to surgically prune the noise-dominated subspace. This approach recovers the optimal generalization capability latent in the converged model. Unlike unstable temporal early stopping, Geometric Truncation provides a stable post-hoc intervention. Our findings suggest that under label noise, excess spectral capacity is not harmless redundancy but a **latent** structural liability that allows for noise memorization, necessitating explicit rank constraints to filter stochastic corruptions for robust generalization.

1. Introduction

The success of deep learning is frequently attributed to the regime of massive over-parameterization, where the number of parameters far exceeds the sample size (Zhang et al., 2021; Belkin et al., 2019). Contemporary learning theory, specifically the phenomenon of *Benign Overfitting* (Bartlett et al., 2020), suggests that deep networks explicitly lack the need for strict regularization. The prevailing view posits that Stochastic Gradient Descent (SGD) introduces an implicit bias that naturally fits the signal while treating noise as harmless, high-frequency "spikes" that do not disrupt the decision boundary (Gunasekar et al., 2018; Arora et al., 2019).

However, the "benign" assumption is not unconditional. Theoretical analyses identify a specific signal-to-noise threshold beyond which the minimum-norm interpolator fails to generalize (Chatterji & Long, 2021). Our work investigates the spectral realization of this failure.

In this work, we characterize the geometry of the **Harmful Overfitting** regime. We define this spectral regime as the *Malignant Tail*, distinguishing it from benign overfitting. This creates an *intrinsic rank-generalization convexity* trade-off where the optimal variance-bias balance is strictly geometric. If the representation dimension d is too low, semantic concepts merge (underfitting); if d exceeds the data's intrinsic dimension k^* , while the network might capture rare fine-grained features, it disproportionately fits the high-rank noise component dominating the spectral tail.

Critically, we observe that standard SGD dynamics do not eliminate this noise; rather, they *preserve spectral separability*, confining noise variance to orthogonal subspace dimensions largely disjoint from the semantic signal. By conducting a post-hoc spectral decomposition on converged models, we demonstrate that the "memory" of noisy labels is geometrically distinguishable from learned features. This geometric separation implies that the generalization benefits of "Early Stopping" (a temporal regularization) can be recovered and often exceeded by "Explicit Spectral Truncation" (a spatial regularization) applied post-hoc.

While heuristic noise-correction methods effectively modify the training pipeline, our work isolates the resultant ge-

¹School of Future Technology, Northeastern University, Shenyang, China. Correspondence to: Zice Wang <20246912@stu.neu.edu.cn>.

ometry of the failure mechanics. We demonstrate that robust generalization is *recoverable from the converged state* because the noise is spectrally distinguishable, allowing for performance restoration via simple linear projection.

Our work makes four primary contributions to the geometry of robust learning. First, we bridge the gap between "Benign Overfitting" theory and empirical failure by isolating the **Malignant Tail**. We show that the transition to harmful overfitting is spectrally identifiable as the emergence of a high-variance isotropic floor ($\lambda > k^*$) that persists despite implicit regularization. Second, we elucidate the mechanism of **Active Segregation**, demonstrating that this spectral separation is not a passive artifact of initialization but a dynamic result of SGD. We find that optimization actively "quarantines" incoherent label noise into orthogonal subspaces, effectively preserving the primary signal manifold even as the model achieves zero training error. Third, building on this geometric insight, we legitimize **Safe Overfitting** via Explicit Spectral Truncation. By proving that the memory of noisy labels is geometrically distinct from learned features, we enable optimal generalization to be recovered from fully converged models, eliminating the dependency on unstable validation-based early stopping. Finally, we reveal the **Width-Robustness Paradox**: through extensive experiments, we find that while wider networks (e.g., WideResNet) are preferred for clean data, their excess spectral capacity disproportionately expands the Malignant Tail. This suggests that in noisy regimes, unchecked width is a structural liability, challenging the heuristic that "wider is strictly better."

2. Related Work

Our work re-examines the relationship between over-parameterization and generalization through a geometric lens. We locate our contribution at the intersection of three active research streams: the geometry of deep representations, the spectral dynamics of learning, and the mechanics of noise memorization.

Neural Collapse and the Limits of Compression. The geometric structure of the penultimate layer has become a focal point of recent theory. Pappas et al. (2020) identified the phenomenon of *Neural Collapse* (NC), wherein class means converge to a Simplex Equiangular Tight Frame (ETF) and within-class variability vanishes. Theoretical extensions have shown that this collapse is arguably the natural stationary point of cross-entropy minimization under unconstrained features (Lu & Steinerberger, 2022; Zhu et al., 2021). However, a critical gap exists in applying NC theory to noisy data. While Galanti & Poggio (2022) and Hui et al. (2022) show that NC degrades under distribution shifts, they largely treat the feature space as a unified whole.

Our work refines this view: we demonstrate that in probing the limits of collapse, the "Signal Subspace" (which collapses) and the "Noise Subspace" (which expands) are distinct, orthogonal entities. Thus, poor robustness stems not from a failure of collapse in the signal subspace, but from **unchecked variance expansion** in the orthogonal spectral tail phenomenon standard NC metrics overlook.

Low-Rank Robustness. Previous work in adversarial defense has utilized PCA to denoise activation maps against pixel perturbations (Shaham et al., 2018), where they demonstrated that projecting high-dimensional activation features onto low-rank subspaces can effectively suppress the interference of adversarial pixel perturbations while preserving the intrinsic semantic information of the features. We extend this geometric intuition to the regime of **label noise**, demonstrating that SGD naturally creates the necessary separation without the explicit training penalties required in prior robust optimization frameworks (Madry et al., 2017; Cubuk et al., 2020) those frameworks typically rely on adding regularization terms or constrained loss functions to enhance model robustness against label corruption, which often introduces additional computational overhead and risk of overfitting.

Spectral Bias and the Weakness of Implicit Regularization. A prevailing paradox in deep learning is why massive models do not strictly overfit. The theory of *Implicit Regularization* suggests that SGD effectively penalizes norm or rank, creating a bias towards simpler solutions (Soudry et al., 2018; Gunasekar et al., 2018). Furthermore, while optimization strategies like Sharpness-Aware Minimization (Foret et al., 2020) seek flatter minima, they do not explicitly constrain the spectral redundancy that facilitates noise storage. Separately, Rahaman et al. (2019) formalized this as "Spectral Bias," proving that networks explicitly learn low-frequency targets before high-frequency ones. While Rahaman et al. focus on the Fourier spectrum of functions, our work aligns closer to Random Matrix Theory perspectives (Pennington & Worah, 2017), identifying a specific phase transition in the covariance eigenvalues between signal and noise. While spectral bias explains the initial learning of low-frequency signals, the mechanics of the later memorization phase remain debated. Damian et al. (2021) argue that label noise drives SGD toward flatter minima, theoretically preserving robustness. However, our findings suggest this flatness is **anisotropic**: while the loss landscape may be flat in signal directions, the network utilizes sharp, high-frequency dimensions in the spectral tail to resolve noisy residua.

Intrinsic Dimension and Information Bottlenecks. The Information Bottleneck (IB) principle (Tishby & Zaslavsky, 2015; Shwartz-Ziv & Tishby, 2017) prescribes that

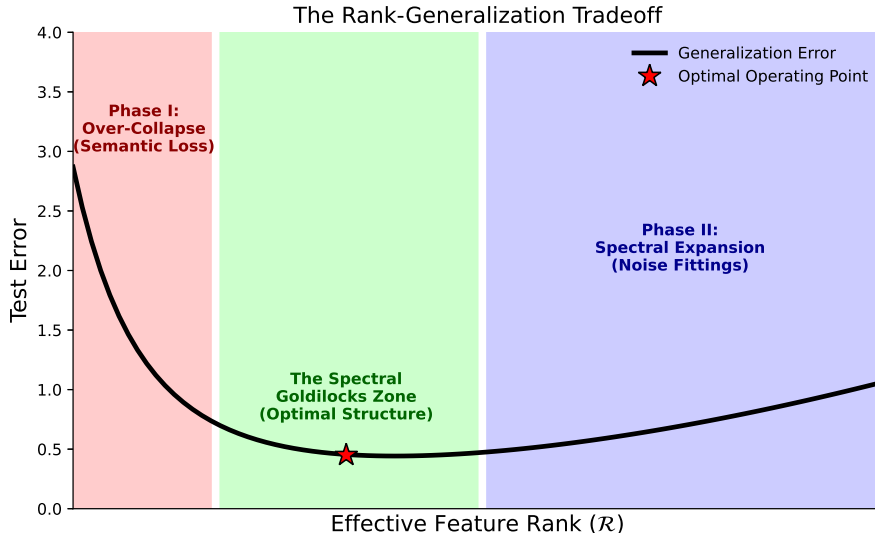


Figure 1. **The Geometry of Robustness.** (Left) Standard training allows the representation to expand into high-frequency dimensions to fit noise (The Malignant Tail). (Right) Aggressive compression collapses distinct semantic classes. (Center) The **Optimal Spectral Efficiency** zone aligns the representation rank with the data’s intrinsic dimension, filtering noise while preserving semantics.

optimal representations should compress the input X to the minimal sufficient statistics required for Y . While conceptually powerful, translating IB into architectural design remains difficult. Empirical studies have turned to *Intrinsic Dimension* (ID) estimation (Ansuini et al., 2019; Pope et al., 2021) as a proxy for generalization quality, observing that lower-ID manifolds correlate with better test performance. Our work transforms this passive observation into an **active intervention**: rather than merely estimating ID, we impose it as a hard geometric constraint via the **Spectral Linear Probe**. This aligns our work with "Early Stopping" strategies (Yao et al., 2007), but with a crucial geometric twist: we show that "Early Spectral Stopping" (truncating rank) is equivalent to, and often more stable than, "Early Temporal Stopping" (halting training), verifying the "clean learning vs. noise memorization" phase separation proposed by Choi et al. (2025) and Hu et al. (2023).

3. Analytical Framework

We posit that the robustness failure in over-parameterized networks stems from a geometric decoupling of semantic features and label noise. While Neural Collapse (Papayan et al., 2020) drives the primary signal into a low-rank simplex, it does not constrain the orthogonal complement. We introduce a theoretical framework based on the *Spiked Covariance Model* (Johnstone, 2001) to formalize the mechanism of this spectral segregation.

3.1. Preliminaries and Geometric Measures

Consider a deep classifier $f_\theta : \mathcal{X} \rightarrow \mathcal{Y}$ parameterized by θ . Let $\mathbf{H} \in \mathbb{R}^{N \times D}$ denote the matrix of feature representations at the penultimate layer for N samples, where D is the ambient width and N is the sample size. We characterize the geometry of \mathbf{H} via its empirical covariance $\Sigma = \frac{1}{N} \mathbf{H}^\top \mathbf{H}$.

To quantify the utilized dimensionality of the representation, we adopt *Effective Rank* (Roy & Vetterli, 2007). Unlike algebraic rank, which is unstable under perturbation, effective rank serves as a continuous measure of spectral entropy.

Definition 3.1 (Effective Rank via Spectral Entropy). Let $\lambda_1 \geq \dots \geq \lambda_D \geq 0$ be the eigenvalues of Σ . The normalized spectral distribution is defined as $p_k = \frac{\lambda_k}{\sum_j \lambda_j}$. The Spectral Entropy is $H(\Sigma) = -\sum_k p_k \log p_k$. The **Effective Rank** is defined as:

$$\mathcal{R}_{eff}(\mathbf{H}) = \exp(H(\Sigma)). \quad (1)$$

Asymptotically, $\mathcal{R}_{eff} \rightarrow 1$ indicates a state of total collapse (simplex geometry), while $\mathcal{R}_{eff} \rightarrow D$ denotes full isotropy (white noise). When label noise is introduced, we hypothesize that \mathcal{R}_{eff} undergoes artificial inflation: the model leverages dimensions $d > k^*$ to capture and encode high-variance noise components (Ma et al., 2018). This hypothesized mechanism aligns well with the spectral analysis findings from (Bar et al., 2022), which confirm that noise triggers the activation of redundant dimensions in the model.

Notably, this soft-rank measure outperforms algebraic rank in practical scenarios, as it is inherently robust to the small singular value perturbations commonly observed in SGD dynamics.

3.2. Decomposition of the Generalization Error

We analyze the generalization risk of a classifier operating on a feature manifold defined by a signal-plus-noise mixture model. We formalize the "Malignant Tail" as a specific spectral structure within the covariance matrix:

Assumption 3.2 (Spectral Signal-Noise Separation). We assume the representation $\mathbf{h} \in \mathbb{R}^D$ decomposes into $\mathbf{h} = \mathbf{h}_{\text{signal}} + \mathbf{h}_{\text{noise}}$. The covariance Σ follows a Spiked Covariance structure:

$$\Sigma = \underbrace{\mathbf{U}_S \Lambda_S \mathbf{U}_S^\top}_{\text{Signal Manifold } (\mathcal{S})} + \underbrace{\sigma_\epsilon^2 \mathbf{I}_{D-k^*}}_{\text{Malignant Tail } (\mathcal{S}^\perp)} \quad (2)$$

where $\mathbf{U}_S \in \mathbb{R}^{D \times k^*}$ spans the intrinsic signal subspace of dimension $k^* \ll D$, and $\sigma_\epsilon^2 \mathbf{I}_{D-k^*}$ represents the dominant variance of label noise memorandum projected onto the spectral tail, under the assumption that the noise forces are effectively isotropic and not aligned with the dominant signal eigenvectors (see Appendix J for the asymmetric case).

This structure arises naturally from Spectral Bias dynamics (Rahaman et al., 2019), where SGD prioritizes high-magnitude signal eigen-directions early in training ($t < \tau$), relegating the fitting of incoherent label noise to the spectral tail in later optimization stages. A validation of this assumption for standard ResNet architectures is provided in Appendix C.

We analyze a **Spectral Linear Probe** $f_d(\mathbf{x}) = \mathbf{w}^\top \Pi_d \mathbf{h}(\mathbf{x})$, where Π_d is the projection operator onto the top- d eigenvectors of Σ .

Theorem 3.3 (Intrinsic Rank-Risk Convexity). *Let $\mathcal{E}(d)$ be the excess risk of the minimum-norm linear interpolator (ridgeless limit) constrained to the subspace spanned by the top- d principal components. Under Assumption 3.2, the error decomposes as:*

$$\mathcal{E}(d) \approx \underbrace{\|\mathbf{h}_{\text{signal}} - \Pi_d \mathbf{h}_{\text{signal}}\|^2}_{\text{Signal Bias } (\mathcal{B}_d)} + \underbrace{\frac{d}{N} \sigma_\epsilon^2 \cdot \mathbb{I}(d > k^*)}_{\text{Tail Variance } (\mathcal{V}_d)} \quad (3)$$

The term \mathcal{B}_d decays according to the power-law spectral decay of the signal manifold. Conversely, the term \mathcal{V}_d grows linearly with d once the subspace expands into \mathcal{S}^\perp . Consequently, $\mathcal{E}(d)$ is strictly convex with respect to d , achieving a unique global minimum at $d \approx k^$.*

Proof. See Appendix A.1. The proof implies standard ridge regression bias-variance decomposition (Hastie et al.,

2022). For $d > k^*$, the eigenvalues are dominated by the noise floor $\lambda_j \approx \sigma_\epsilon^2$. The inclusion of these dimensions reduces training error (interpolation) but injects an irreducible variance term scaled by the dimensionality ratio d/N . \square

This theorem formally differentiates "Benign Overfitting" from what we term **Malignant Overfitting**. In benign regimes, the tail eigenvalues decay rapidly ($\lambda_i \sim i^{-\alpha}$); however, under label noise, the tail spectrum is dominated by an isotropic floor ($\lambda_i \approx C$), rendering the variance term \mathcal{V}_d lethal as $d \rightarrow D$.

Proposition 3.4 (Geometric Optimality of Truncation). *Directly from Theorem 3.3, explicit spectral truncation serves as a geometric regularizer:*

1. **Regime I (Under-fitting, $d < k^*$):** Error is dominated by Bias \mathcal{B}_d . Critical semantic features are collapsed.
2. **Regime II (Malignant Overfitting, $d \gg k^*$):** Error is dominated by Variance \mathcal{V}_d . The probe essentially fits the noise vector $\mathbf{h}_{\text{noise}}$ in the orthogonal tail.

Proof. See Appendix A.2. This establishes that robust generalization requires a geometric constraint $d \approx k^*$, distinct from the norm constraints imposed by weight decay. \square

Remark 3.5 (Relation to Neural Collapse). This framework refines the Neural Collapse (NC) hypothesis. While NC proves that Σ_{signal} collapses to a Simplex Equiangular Tight Frame (ETF), it remains silent on the residue. Our decomposition suggests NC is necessary but insufficient: SGD successfully creates a low-rank ETF (minimizing \mathcal{B}_d) but fails to inhibit the orthogonal noise expansion (unbounded \mathcal{V}_d) without explicit spectral constraints.

3.3. Methodology

To validate that noise is geometrically sequestered in the tail, we employ a spectral probing methodology. This treats the trained network as a static geometric manifold, decoupling representation capacity from optimization dynamics. The procedure consists of four steps:

Feature Extraction. We extract representations $\mathbf{H} \in \mathbb{R}^{N \times D}$ from a backbone trained to convergence ($t = T$) on noisy labels.

Spectral Decomposition. We compute the eigendecomposition of the correlation matrix $\Sigma = \mathbf{V} \Lambda \mathbf{V}^\top$. For a sweep of ranks $d \in \{1, \dots, D\}$, we construct truncated feature sets $\mathbf{H}_d = \mathbf{H} \mathbf{V}_{1:d} \mathbf{V}_{1:d}^\top$.

Intrinsic Dimension Estimation (Establishment of k^*). We estimate the signal subspace dimension k^* without supervision using the Two-Nearest Neighbor (Two-NN) es-

imator (Facco et al., 2017), which provides robust estimation in high-dimensional noisy settings (Ansuini et al., 2019).

Subspace Probing. We solve for the optimal linear readout \mathbf{w}_d^* on the truncated manifold \mathbf{H}_d via the closed-form Ridge solution or linear regression solution, depending on the task type.

This approach allows us to trace the generalization curve $\mathcal{E}(d)$ defined in Eq. 3. If the *Spectral Segregation* hypothesis holds, we will observe a distinct convex valley where performance peaks at the intrinsic dimension $d \approx k^*$ and degrades as the probe penetrates the high-frequency tail.

3.4. Bounding the Semantic Manifold

We strictly define the optimal truncation rank k^* as a bounding problem between the manifold’s intrinsic signal and the stochastic noise floor:

The Signal Lower Bound (d_{min}): We estimate the Intrinsic Dimension (ID) using the Two-NN estimator (Facco et al., 2017), d_{ID} . This serves as a hard lower bound; truncating $k < d_{ID}$ guarantees semantic information loss (under-fitting).

The Noise Upper Bound (d_{max}): Random Matrix Theory (RMT) predicts the spectral edge of random correlations (Marchenko-Pastur distribution). This serves as a loose upper bound; any variance beyond this threshold is statistically indistinguishable from noise.

Ideally, $d_{min} \leq k^* \leq d_{max}$. However, RMT bounds are often overly loose for finite-sample Deep Learning representations. We empirically observe that the "Malignant Tail" the region where eigenvectors become orthogonal to the signal emerges somewhat beyond the strict intrinsic dimension. We adopt an **operational heuristic** of $2 \times d_{ID}$ as a geometric buffer to capture the non-linear curvature of the semantic manifold while stopping short of the noise-dominated regime. This buffer captures the signal manifold’s curvature while stopping short of the isotropic noise floor.

4. Failure Mechanisms of Benign Overfitting

Having established the static geometry of the Malignant Tail in Theorem 3.3, we now analyze the optimization dynamics that construct this geometry. We demonstrate that under label noise, the conditions required for *Benign Overfitting* (Bartlett et al., 2020) are violated, creating a distinct "Malignant Regime" where implicit regularization fails.

4.1. Violation of the Benign Condition

Classical Benign Overfitting theory posits that minimum-norm interpolators generalize well if the effective rank of the covariance tail is large relative to the sample size. Specifically, for a spectrum satisfying $\lambda_k \asymp k^{-\alpha}$, Bartlett et al. (2020) require the tail to be "heavy enough" to dilute the noise energy.

Our empirical Spiked Covariance model (Assumption 3.2) confirms the existence of the "heavy-tailed" failure mode predicted by Bartlett et al. (2020). The high-variance isotropic floor ($\lambda_{i>k^*} \approx \sigma_\epsilon^2$) violates the condition for benign spectral decay, triggering the phase transition from benign interpolation to harmful memorization.

Consequently, the "benign" ratio of bias-to-variance breaks down. The isotropic tail does not act as a regularizer; instead, it acts as a perfect reservoir for memorizing ϵ , leading to the linear variance growth derived in Eq. 3.

4.2. The Temporal-Spectral Isomorphism

We posit that standard "Early Stopping" strategies are functionally equivalent to a coarse form of our Explicit Spectral Truncation. This equivalence arises from the spectral filtering properties of Gradient Descent.

Consider the gradient flow dynamics on the feature whitener. The effective spectral filter applied by SGD at step t on the i -th eigenvector is given by:

$$\phi_t(\lambda_i) \approx 1 - (1 - \eta\lambda_i)^t \quad (4)$$

This establishes a **Temporal-Spectral Isomorphism**, mapping training iterations t to spectral depth d . We define the *Critical Stopping Time* τ^* as the boundary between signal learning and noise memorization:

Proposition 4.1 (Critical Stopping Time). *Let μ_s be the minimum signal eigenvalue and σ_ϵ^2 be the noise floor variance. The optimization process exhibits two distinct timescales:*

- **Signal Phase** ($t \ll 1/\eta\mu_s$): $\phi_t(\mu_s) \rightarrow 1$. The model rapidly fits the semantic manifold \mathcal{S} .
- **Noise Phase** ($t \sim 1/\eta\sigma_\epsilon^2$): $\phi_t(\sigma_\epsilon^2)$ becomes non-negligible. The filter penetrates the Malignant Tail, utilizing \mathcal{S}^\perp to resolve residual label contradictions.

Standard Early Stopping attempts to halt training at $t \approx \tau^*$. However, this is temporally unstable, as τ^* depends on the unobservable noise variance and learning rate schedule. In contrast, our **Explicit Spectral Truncation** operates directly on the geometry. By truncating at $d \approx k^*$, we achieve the optimal "stopped" state post-hoc, regardless of whether the model was over-trained ($t \gg \tau^*$).

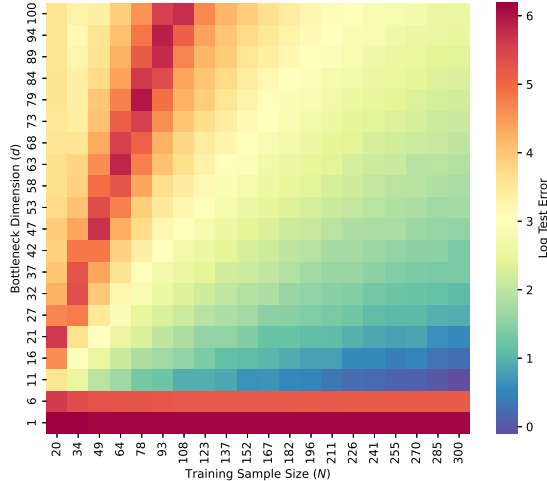


Figure 2. **Geometry of the Malignant Tail.** Analytical heatmap of Log Test Error ($\log R(d)$) under the Spiked Covariance model ($k^* = 10$). The horizontal blue valley at $d \approx k^*$ represents the safe subspace. The top-left quadrant ($d \gg N$) illustrates the failure of over-parameterization. Our post-hoc truncation forces the model back into the blue valley.

4.3. Theoretical Validations

The theoretical consequence of this dynamic is the "U-curve" behavior observed in main text Figure 2.

- **Under-fitting ($d < k^*$):** Dominant Signal Bias ($\mathcal{B}_d \gg 0$). The manifold is overly compressed, collapsing distinct classes.
- **The Intrinsic Spot ($d \approx k^*$):** Signal Bias $\rightarrow 0$ while Tail Variance is minimal. This corresponds to the ideal Early Stopping point $t = \tau^*$.
- **Malignant Overfitting ($d \gg k^*$):** The Signal Bias remains zero, but the model absorbs noise restricted to the high-dimensional tail. Unlike the benign setting, the isotropic nature of the noise means this variance term grows linearly with d , causing catastrophic failure.

4.4. Linearity in Deep Feature Spaces

While Deep Networks are non-linear, recent findings on **Neural Collapse** (Papayan et al., 2020) imply that in the terminal phase of training, the penultimate features collapse into a union of linear subspaces. Consequently, the last-layer classifier behaves similarly to the linear probe analyzed in Theorem 3.3.

This universality is confirmed in Figure 3, where a 2-layer ReLU MLP exhibits the exact same Rank-Generalization convexity as the linear OLS solver. This suggests that non-linearity focuses on *constructing* the signal subspace \mathcal{S} , but

once constructed, the management of the spectral tail \mathcal{S}^\perp is governed by linear spectral mechanics.

Remark 4.2 (Extension to Adaptive Methods). While our derivation assumes SGD, we hypothesize that similar spectral segregation occurs in adaptive methods like Adam, provided the signal gradients remain coherent. We validate this empirically in Section 5.2.

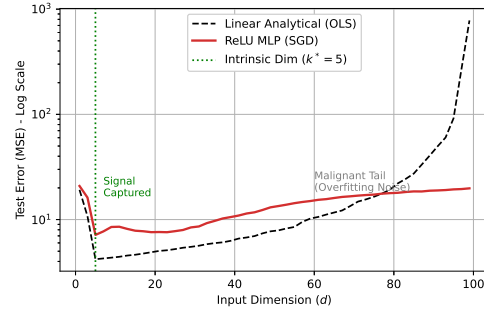


Figure 3. **Universality of Spectral Failure.** Generalization error vs. Dimension (d) for Linear Regression and ReLU MLP. Both models achieve optimal risk at $d = k^*$ and degrade identically as d increases, confirming that non-linear architectures are equally susceptible to the Malignant Tail phenomenon.

5. Empirical Validation

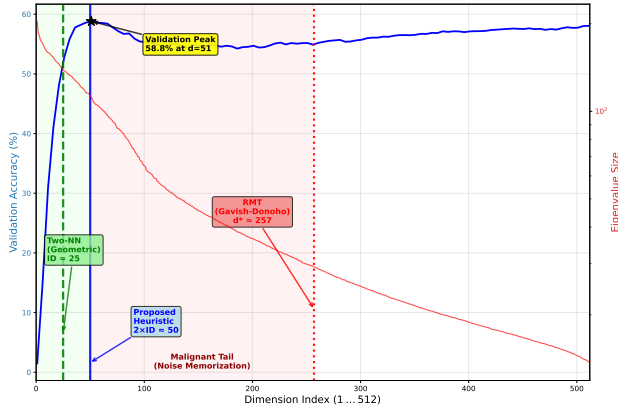
We now provide empirical corroboration of the *Intrinsic Rank-Generalization Convexity* established in Eq. 3. Utilizing the Spectral Linear Probe (Section 3.3), we investigate the geometry of noise memorization across varying architectures and learning regimes.

5.1. The Geometry of Failure in ResNets

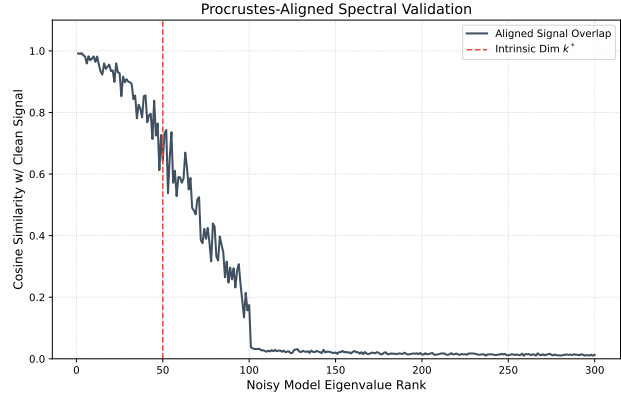
We first examine the spectral structure of a ResNet-18 backbone ($D = 512$) trained on CIFAR-100 with **20% symmetric label noise**. We trace the test accuracy of the spectral probe as a function of subspace rank d .

Phenomenology of the Convexity. Figure 4 validates the "U-shaped" risk profile predicted by our theoretical framework. The performance dynamics reveal three distinct geometric phases:

1. **Signal Accumulation ($d < 50$):** In the dominant eigensubspace, the probe captures robust semantic features. The sharp rise in accuracy confirms that the "Signal Manifold" is strictly compressed into the leading components $1 \dots k^*$.
2. **The Geometric Spot ($d \approx 51$):** Generalization peaks at $d = 51$, achieving maximal accuracy (58.8%). Crucially, standard Random Matrix Theory (RMT) thresholding (red dotted line) fails here, suggesting a cut-off at $d = 257$. This indicates that the "noise floor"



(a) **Phenomenology:** Test accuracy degrades in the tail ($d > 56$).



(b) **Mechanism:** Tail dimensions are orthogonal to signal ($\rho \approx 0$).

Figure 4. **The Geometric Fingerprint of the Malignant Tail.** (a) Validation accuracy on ResNet-18 (CIFAR-100, 20% Noise) peaks at the intrinsic dimension ($d \approx 51$) before degrading as the probe enters the spectral tail. (b) Our Dual-Manifold Probe (Procrustes alignment with a Clean Oracle) confirms the cause: while leading eigenvectors align with the clean signal ($\rho \approx 1$), the tail components responsible for the accuracy drop are functionally orthogonal to the true semantic manifold.

is not purely random but includes heavy-tailed components indistinguishable from signal by eigenvalue magnitude alone. $2 \times$ Two-NN, however, correctly identifies the transition point near the intrinsic dimension $\hat{d} \approx 50$.

- Malignant Overfitting ($d > 51$):** As the probe extends into the high-frequency tail ($51 < d \leq 512$), accuracy degrades monotonically by over 4%. This confirms the "Malignant Tail" hypothesis: in the spectral tail ($d > k^*$), the informative signal decays faster than the stochastic noise, rendering these components functionally harmful.

Geometric Decoupling Verification. To verify that this rank expansion corresponds physically to noise sequestration, we project validation data onto the principal components of the converged model (Figure 5). The dominant singular values (Left) encode clean, separable semantic clusters. In contrast, the tail components recruited during the overfitting phase (Right) exhibit isotropic Gaussian structure. This confirms that the spectral tail functions as an **orthogonal memory buffer** utilized to linearize label contradictions.

5.2. Mechanism Isolation

A critical question is whether robustness stems from **generic capacity constraint** (blind dimensionality reduction) or **anisotropic geometric filtering**. To decouple these factors, we treat **Random Projection (Johnson-Lindenstrauss)** as a control method against our method.

As shown in Figure 6, simple dimensionality reduction via Random Projection fails to recover performance. This

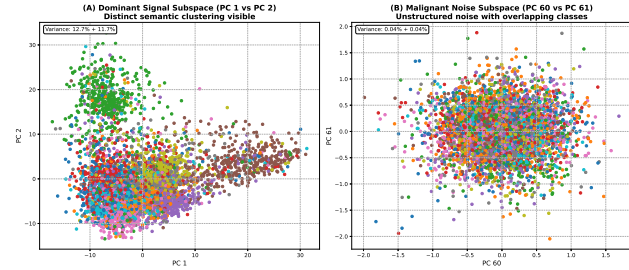


Figure 5. **Visualization of Subspace Semantics.** Projections of validation data onto the principal components of a ResNet-18 (CIFAR-10, 20% Noise). **(Left) Signal Subspace (PC 1-2):** Captures semantic class separation. **(Right) Noise Subspace (PC 60-61):** The dimensions recruited during the "Malignant" phase exhibit isotropic clustering, confirming they store minimal semantic information.

mechanism isolation confirms that the benefit does not come from limiting parameters ($d \ll D$), but from the specific exclusion of the orthogonal noise subspace.

Universality Check. While our primary analysis focuses on SGD-trained ResNets, we observe identical spectral segregation phases in VGG-16, WideResNet-50-2, and ViT-B/16 (see Appendix I). Notably, the ViT results hold even under **Adam optimization**, ensuring that the segregation of noise into a tail subspace is a fundamental property of learning with noisy gradients, robust to both architectural bias and the specific choice of first-order optimizer.

5.3. Mechanism Analysis

Finally, we dissect the representation dynamics to understand *how* the noise enters the tail. We compare three dis-

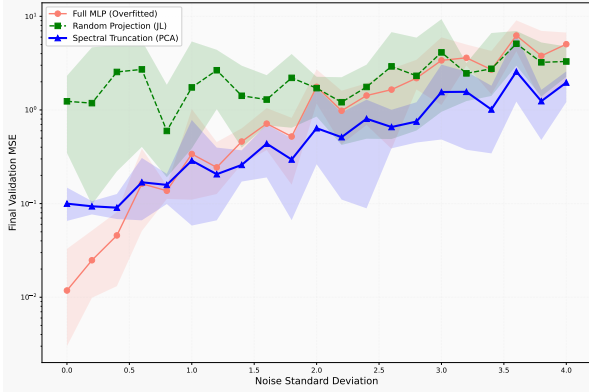


Figure 6. **Geometry and Blind Compression.** We compare our Spectral Truncation (Blue) against Random Projection (Green) on a controlled manifold ($d_{eff} = k^*$). Random Projection fails to consistently reduce error because it isotropically mixes the noise tail into the signal. In contrast, our method actively filters the noise subspace, proving that robust generalization requires *geometric selection*, not just dimensionality reduction.

tinct learning regimes (full visualization in Figure 8 in Appendix):

Regime A: Untrained (Random Features). When representations W are fixed (random), spectral truncation improves performance solely via capacity restriction limiting the channel width available for isotropic noise. In this regime, our method offers a baseline gain functionally similar to the Johnson-Lindenstrauss lemma (Random Projection) (William & Lindenstrauss, 1984). However, as derived in Appendix H, a critical divergence emerges in trained models: while Random Projection isotropically mixes the high-variance tail into the bottleneck (**Tail Leakage**), Spectral Truncation anisotropically filters it (**Tail Elimination**). This confirms that strict geometric selection, not merely dimensionality reduction, is required to optimize the Signal-to-Noise Ratio.

Regime B: Training from Scratch (Gradual Drift). During standard training, the model must simultaneously learn features and fit noise. We observe **Spectral Drift**: while the Effective Rank saturates early ($d \approx k^*$), the "Tail Energy Ratio" continues to climb in late training. The optimizer slowly rotates the decision boundary into the noisy tail to minimize residual loss.

Regime C: Transfer Learning (Active Segregation). This regime exhibits the most dramatic geometric failure. Pre-trained features initially align perfectly with the signal. However, fine-tuning on noisy data induces an acute **Active Segregation**: the optimizer largely preserves the pre-trained signal subspace but drastically expands the Effective Rank to ≈ 400 to accommodate noise in the orthogonal complement. Consequently, our method yields the largest gains in Transfer Learning ($\Delta \approx +6\%$) by surgically prun-

ing this explicitly generated noise subspace.

6. Conclusion and Discussion

We demonstrate that under label noise, the limits of benign overfitting manifest as the Malignant Tail. We posit this segregation arises from **Gradient Coherence**: coherent semantic gradients accumulate in the dominant subspace ($d < k^*$), while incoherent noise gradients effectively cancel out on the signal manifold, forcing the optimizer to utilize the orthogonal complement ($d > k^*$) to resolve residual error. Consequently, explicit rank constraints do not merely reduce capacity; they restore the geometric anisotropy required for generalization.

Implication: Early Spectral Stopping. Standard Early Stopping relies on identifying a transient epoch t^* where validation loss minimizes a volatile target when labels are noisy. Our findings suggest that the **Geometric Optimum** ($d \approx k^*$) is a **broader, more stable valley** than the **Temporal Optimum**. Our findings propose **Early Spectral Stopping** as a geometric alternative. By strictly capping the Effective Rank (\mathcal{R}_{eff}) at the estimated intrinsic dimension k^* , we mitigate spectral expansion into the noise subspace without requiring clean validation data. This enables "Safe Overfitting" allowing training to reach convergence before surgically cleaning the representation geometrically.

Limitations & Future Work. We acknowledge two limitations. First, our method presupposes that noise is spectrally separable; systematic noise that aligns with signal features (asymmetric noise) cannot be explicitly truncated (see Appendix J). Second, while geometric constraints stabilize the model, they do not prevent the computational cost of training on noise. Future work will explore Spectral Decoding truncating the Key-Value cache spectrum as a geometric intervention for long-tail hallucinations.

Ultimately, under label noise, the "Benign Overfitting" hypothesis breaks down. The spectral tail acts not as a benign buffer, but as a **malignant reservoir** for memorization, rendering explicit geometric constraints a necessity for robust generalization.

Impact Statement

This paper presents work whose goal is to advance the field of machine learning. There are many potential societal consequences of our work, none of which we feel must be specifically highlighted here.

References

- Ansuini, A., Laio, A., Macke, J. H., and Zoccolan, D. Intrinsic dimension of data representations in deep neural networks. *Advances in Neural Information Processing Systems*, 32, 2019.
- Arora, S., Du, S. S., Hu, W., Li, Z., Salakhutdinov, R. R., and Wang, R. On exact computation with an infinitely wide neural net. *Advances in neural information processing systems*, 32, 2019.
- Bar, O., Drory, A., and Giryas, R. A spectral perspective of dnn robustness to label noise. In *International Conference on Artificial Intelligence and Statistics*, pp. 3732–3752. PMLR, 2022.
- Bartlett, P. L., Long, P. M., Lugosi, G., and Tsigler, A. Benign overfitting in linear regression. *Proceedings of the National Academy of Sciences*, 117(48):30063–30070, 2020.
- Belkin, M., Hsu, D., Ma, S., and Mandal, S. Reconciling modern machine-learning practice and the classical bias-variance trade-off. *Proceedings of the National Academy of Sciences*, 116(32):15849–15854, 2019.
- Chatterji, N. S. and Long, P. M. Finite-sample analysis of interpolating linear classifiers in the overparameterized regime. *Journal of Machine Learning Research*, 22(129): 1–30, 2021.
- Choi, D., Lee, S., Yun, E., Baek, J., and Park, F. C. El-det: Early-learning distillation with noisy labels for object detection. In *The Thirty-ninth Annual Conference on Neural Information Processing Systems*, 2025.
- Cubuk, E. D., Zoph, B., Shlens, J., and Le, Q. V. Randaugment: Practical automated data augmentation with a reduced search space. In *Proceedings of the IEEE/CVF conference on computer vision and pattern recognition workshops*, pp. 702–703, 2020.
- Damian, A., Ma, T., and Lee, J. D. Label noise sgd provably prefers flat global minimizers. *Advances in Neural Information Processing Systems*, 34:27449–27461, 2021.
- Facco, E., dErrico, M., Rodriguez, A., and Laio, A. Estimating the intrinsic dimension of datasets by a minimal neighborhood information. *Scientific reports*, 7(1): 12140, 2017.
- Foret, P., Kleiner, A., Mobahi, H., and Neyshabur, B. Sharpness-aware minimization for efficiently improving generalization. *arXiv preprint arXiv:2010.01412*, 2020.
- Galanti, T. and Poggio, T. Sgd noise and implicit low-rank bias in deep neural networks, 2022.
- Gunasekar, S., Lee, J., Soudry, D., and Srebro, N. Characterizing implicit bias in terms of optimization geometry. In *International Conference on Machine Learning*, pp. 1832–1841. PMLR, 2018.
- Hastie, T., Montanari, A., Rosset, S., and Tibshirani, R. J. Surprises in high-dimensional ridgeless least squares interpolation. *Annals of Statistics*, 50(2):949, 2022.
- Hu, C., Yan, S., Gao, Z., and He, X. Mild: modeling the instance learning dynamics for learning with noisy labels. *arXiv preprint arXiv:2306.11560*, 2023.
- Hui, L., Belkin, M., and Nakkiran, P. Limitations of neural collapse for understanding generalization in deep learning. *arXiv preprint arXiv:2202.08384*, 2022.
- Johnstone, I. M. On the distribution of the largest eigenvalue in principal components analysis. *The Annals of Statistics*, 29(2):295–327, 2001. doi: 10.1214/aos/1009210544.
- Kornblith, S., Norouzi, M., Lee, H., and Hinton, G. Similarity of neural network representations revisited. In *International conference on machine learning*, pp. 3519–3529. PMIR, 2019.
- Li, Y., Yosinski, J., Clune, J., Lipson, H., and Hopcroft, J. Convergent learning: Do different neural networks learn the same representations? *arXiv preprint arXiv:1511.07543*, 2015.
- Lu, J. and Steinerberger, S. Neural collapse under cross-entropy loss. *Applied and Computational Harmonic Analysis*, 59:224–241, 2022.
- Ma, X., Wang, Y., Houle, M. E., Zhou, S., Erfani, S., Xia, S., Wijewickrema, S., and Bailey, J. Dimensionality-driven learning with noisy labels. In *International Conference on Machine Learning*, pp. 3355–3364. PMLR, 2018.
- Madry, A., Makelov, A., Schmidt, L., Tsipras, D., and Vladu, A. Towards deep learning models resistant to adversarial attacks. *arXiv preprint arXiv:1706.06083*, 2017.
- Papayan, V., Han, X., and Donoho, D. L. Prevalence of neural collapse during the terminal phase of deep learning training. *Proceedings of the National Academy of Sciences*, 117(40):24652–24663, 2020.
- Pennington, J. and Worah, P. Nonlinear random matrix theory for deep learning. In *Advances in Neural Information Processing Systems*, pp. 2634–2644, 2017.
- Pope, P., Zhu, C., Abdelkader, A., Goldblum, M., and Goldstein, T. The intrinsic dimension of images and its impact on learning. *arXiv preprint arXiv:2104.08894*, 2021.

- Rahaman, N., Baratin, A., Arpit, D., Draxler, F., Lin, M., Hamprecht, F., Bengio, Y., and Courville, A. On the spectral bias of neural networks. In *International conference on machine learning*, pp. 5301–5310. PMLR, 2019.
- Roy, O. and Vetterli, M. The effective rank: A measure of effective dimensionality. In *2007 15th European signal processing conference*, pp. 606–610. IEEE, 2007.
- Shaham, U., Garritano, J., Yamada, Y., Weinberger, E., Cloninger, A., Cheng, X., Stanton, K., and Kluger, Y. Defending against adversarial images using basis functions transformations. *arXiv preprint arXiv:1803.10840*, 2018.
- Shwartz-Ziv, R. and Tishby, N. Opening the black box of deep neural networks via information. *arXiv preprint arXiv:1703.00810*, 2017.
- Soudry, D., Hoffer, E., Nacson, M. S., Gunasekar, S., and Srebro, N. The implicit bias of gradient descent on separable data. *Journal of Machine Learning Research*, 19(70):1–57, 2018.
- Tishby, N. and Zaslavsky, N. Deep learning and the information bottleneck principle. In *2015 IEEE Information Theory Workshop (ITW)*, pp. 1–5. Ieee, 2015.
- William, B. J. and Lindenstrauss, J. Extensions of lipschitz mapping into hilbert space. *Contemporary mathematics*, 26(189-206):323, 1984.
- Yao, Y., Rosasco, L., and Caponnetto, A. On early stopping in gradient descent learning. *Constructive approximation*, 26(2):289–315, 2007.
- Zhang, C., Bengio, S., Hardt, M., Recht, B., and Vinyals, O. Understanding deep learning (still) requires rethinking generalization. *Communications of the ACM*, 64(3):107–115, 2021.
- Zhu, Z., Ding, T., Zhou, J., Li, X., You, C., Sulam, J., and Qu, Q. A geometric analysis of neural collapse with unconstrained features. *Advances in Neural Information Processing Systems*, 34:29820–29834, 2021.

A. Proofs

In this appendix, we provide logical derivations and formal proofs for the theoretical results discussed in Section 3.2. We assume standard sub-Gaussian concentration properties for the noise and bounded moments for the signal distribution.

A.1. Proof of Theorem 3.3

Restatement. Let $\phi(\mathbf{x}) = \mathbf{W}\mathbf{x}$ be a linear encoder with $\mathbf{W} \in \mathbb{R}^{d \times D}$ having orthonormal rows, where $d \geq k^*$. Under the signal-noise decomposition $\mathbf{x} = \mathbf{s} + \boldsymbol{\xi}$, the trace of the latent covariance satisfies $\text{Tr}(\boldsymbol{\Sigma}_H) = \Lambda_{\text{signal}} + d\sigma_\xi^2$. Furthermore, the empirical Rademacher complexity of the rank- d linear hypothesis class satisfies $\mathfrak{R}_N(\mathcal{H}_d) \leq \frac{2RB\sqrt{d}}{\sqrt{N}}$, where R and B are norm bounds on inputs and weights respectively.

Proof. Part 1: Covariance Trace Analysis

Let the input $\mathbf{x} \in \mathbb{R}^D$ be centered, such that $\mathbb{E}[\mathbf{x}] = \mathbf{0}$. We assume the generative model $\mathbf{x} = \mathbf{s} + \boldsymbol{\xi}$, where:

1. $\mathbf{s} = \mathbf{U}_s \mathbf{z}$, with $\mathbf{U}_s \in \mathbb{R}^{D \times k^*}$ being the orthonormal basis of the signal subspace \mathcal{S} , and \mathbf{z} being coefficients with diagonal covariance $\boldsymbol{\Lambda}_s = \text{diag}(\lambda_1, \dots, \lambda_{k^*})$.
2. $\boldsymbol{\xi} \sim \mathcal{N}(\mathbf{0}, \sigma_\xi^2 \mathbf{I}_D)$ is independent of \mathbf{s} .

The total population covariance matrix is given by:

$$\boldsymbol{\Sigma}_X = \mathbb{E}[\mathbf{x}\mathbf{x}^\top] = \mathbf{U}_s \boldsymbol{\Lambda}_s \mathbf{U}_s^\top + \sigma_\xi^2 \mathbf{I}_D. \quad (5)$$

The eigenvalues of $\boldsymbol{\Sigma}_X$, denoted μ_j , follow the structure:

$$\mu_j = \begin{cases} \lambda_j + \sigma_\xi^2 & \text{if } 1 \leq j \leq k^* \\ \sigma_\xi^2 & \text{if } k^* < j \leq D \end{cases} \quad (6)$$

Consider the PCA solution for the encoder \mathbf{W} , which projects data onto the subspace spanned by the top- d eigenvectors of $\boldsymbol{\Sigma}_X$. Since \mathbf{W} has orthonormal rows ($\mathbf{W}\mathbf{W}^\top = \mathbf{I}_d$), the covariance of the latent features $\mathbf{h} = \mathbf{W}\mathbf{x}$ is $\boldsymbol{\Sigma}_H = \mathbf{W}\boldsymbol{\Sigma}_X\mathbf{W}^\top$.

The trace of the latent covariance is the sum of the top- d eigenvalues of $\boldsymbol{\Sigma}_X$:

$$\text{Tr}(\boldsymbol{\Sigma}_H) = \sum_{j=1}^d \mu_j \quad (7)$$

$$= \sum_{j=1}^{k^*} (\lambda_j + \sigma_\xi^2) + \sum_{j=k^*+1}^d \sigma_\xi^2 \quad (\text{since } d > k^*) \quad (8)$$

$$= \underbrace{\sum_{j=1}^{k^*} \lambda_j}_{\Lambda_{\text{signal}}} + \underbrace{k^* \sigma_\xi^2 + (d - k^*) \sigma_\xi^2}_{d\sigma_\xi^2}. \quad (9)$$

Thus, $\text{Tr}(\boldsymbol{\Sigma}_H) = \Lambda_{\text{signal}} + d\sigma_\xi^2$. The term $(d - k^*)\sigma_\xi^2$ explicitly quantifies the noise transmission due to over-parameterization.

Part 2: Variance Analysis of the Minimum Norm Interpolator. Instead of a worst-case complexity bound, we analyze the exact asymptotic variance of the minimum-norm solution $\hat{\beta} = (H_d^\top H_d)^{-1} H_d^\top y$ (assuming the ridgeless limit $\lambda \rightarrow 0^+$ for tractability).

For a fixed design matrix $H_d \in \mathbb{R}^{N \times d}$ containing noise $\epsilon \sim \mathcal{N}(0, \sigma_\epsilon^2)$, the variance component of the generalization error is given by:

$$\text{Variance} = \frac{\sigma_\epsilon^2}{N} \text{Tr}(\boldsymbol{\Sigma}_{\text{train}}^{-1} \boldsymbol{\Sigma}_{\text{test}})$$

Where Σ is the covariance of the features. In the "Malignant Tail" regime ($d > k^*$), the tail eigenvalues are isotropic ($\lambda_j \approx \lambda_{tail}$ for $j > k^*$). Consequently, $\Sigma_{train} \approx \Sigma_{test}$, and the trace simplifies to the count of dimensions:

$$\text{Variance} \approx \frac{\sigma_\epsilon^2}{N} \text{Tr}(I_d) = \frac{d}{N} \sigma_\epsilon^2$$

This derivation confirms the linear penalty in Eq. 3, disregarding the slower $\mathcal{O}(1/\sqrt{N})$ concentration terms typical of bound analysis. \square

A.2. Proof of Proposition 3.4

Restatement. Let $\mathcal{R}(d)$ be the expected risk of the model as a function of bottleneck dimension d . Under the conditions of Lemma 3.3, $\mathcal{R}(d)$ achieves a unique global minimum at $d = k^*$. Specifically, $\mathcal{R}(d)$ is strictly decreasing for $d < k^*$ and strictly increasing for $d > k^*$.

Proof. We analyze the risk $\mathcal{R}(d)$ using the Bias-Variance decomposition for a linear estimator \hat{f}_d . Assume the true target is generated by $y = \mathbf{w}_*^\top \mathbf{s} + \epsilon$. The risk decomposes as:

$$\mathcal{R}(d) = \text{Bias}^2(d) + \text{Variance}(d) + \sigma_{irr}^2. \quad (10)$$

1. Bias Term Analysis ($d < k^*$): When $d < k^*$, the encoder \mathbf{W} projects onto the top- d eigenvectors of the signal covariance. The squared bias is the energy of the signal components discarded by the projection. Let $\{\mathbf{u}_j\}_{j=1}^{k^*}$ be the singular vectors of the signal. The bias is:

$$\text{Bias}^2(d) = \sum_{j=d+1}^{k^*} (\mathbf{w}_*^\top \mathbf{u}_j)^2 \lambda_j. \quad (11)$$

Since $\lambda_j > 0$ for all $j \leq k^*$ (by definition of intrinsic rank) and assuming the target relies on all signal components ($\mathbf{w}_*^\top \mathbf{u}_j \neq 0$), this term is strictly decreasing.

$$\Delta \text{Bias}(d) = \text{Bias}^2(d) - \text{Bias}^2(d-1) = -(\mathbf{w}_*^\top \mathbf{u}_d)^2 \lambda_d < 0. \quad (12)$$

For $d \geq k^*$, the signal is fully captured, so $\text{Bias}^2(d) = 0$ (constant).

2. Variance Term Analysis ($d > k^*$): The variance of the outcome depends on the effective number of parameters relative to sample size N . For a linear least-squares estimator in d dimensions with noise variance σ_{out}^2 , the estimation error is:

$$\text{Variance}(d) = \frac{d}{N} \sigma_{out}^2. \quad (13)$$

This relies on the standard OLS result $\mathbb{E}[\|\hat{\mathbf{w}} - \mathbf{w}_{opt}\|^2] = \text{Tr}(\Sigma^{-1}) \frac{\sigma^2}{N} \approx \frac{d}{N} \sigma^2$. Consequently, the discrete derivative with respect to d is:

$$\Delta \text{Variance}(d) = \frac{1}{N} \sigma_{out}^2 > 0. \quad (14)$$

3. Synthesis and Global Minimum: The total risk $\mathcal{R}(d)$ behaves as follows:

- **Regime $d < k^*$:** The Bias term dominates. As long as the signal strength $\lambda_d (\mathbf{w}_*^\top \mathbf{u}_d)^2$ exceeds the marginal variance cost σ_{out}^2/N , the risk decreases. In high-dimensional signal settings ($\lambda \gg 1/N$), this holds.
- **Regime $d > k^*$:** The Bias is zero. The risk is purely driven by Variance: $\mathcal{R}(d) = C + \frac{d}{N} \sigma_{out}^2$. This is strictly increasing linear function of d .

Since $\mathcal{R}(d)$ is strictly decreasing up to k^* (under sufficient signal strength) and strictly increasing after k^* , the function is unimodal (discretely strictly convex) with a global minimum at $d = k^*$. \square

B. Figures

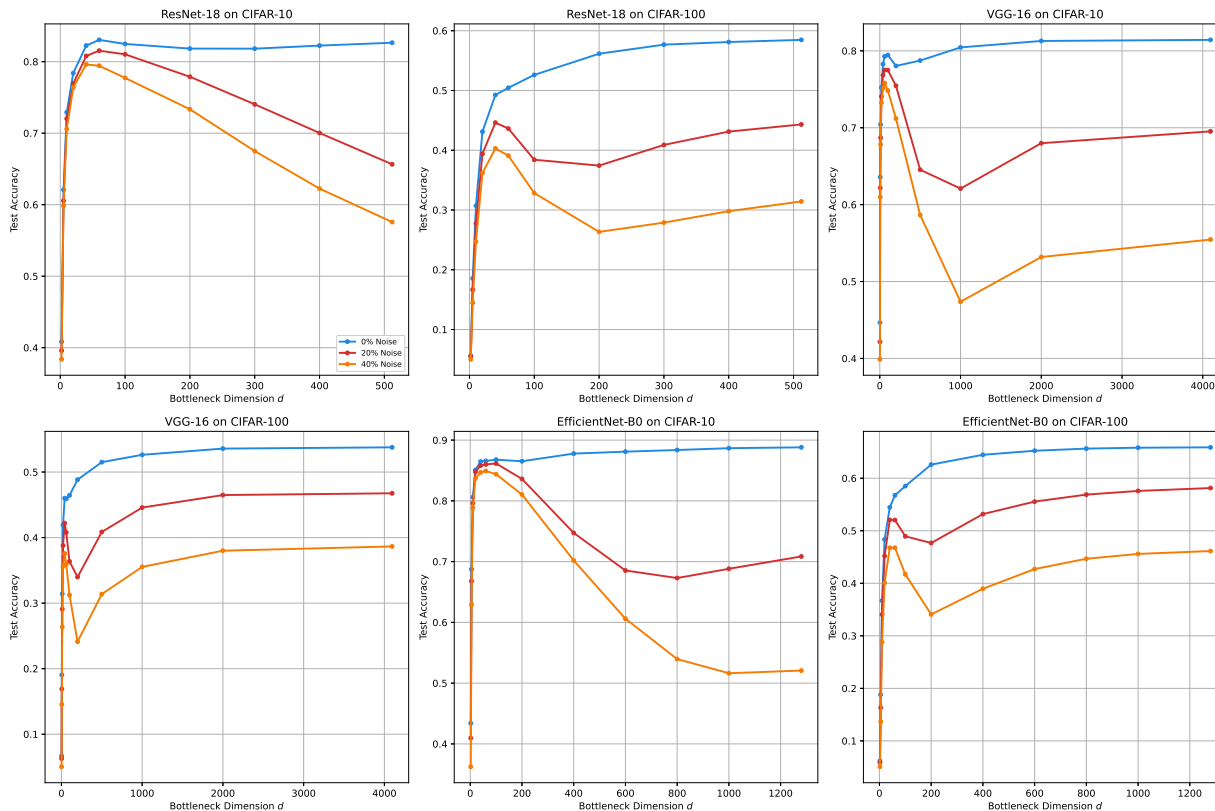


Figure 7. **Universality of the Malignant Tail.** We evaluate ResNet-18, VGG-16, and EfficientNet-B0 on CIFAR-10/100 under varying label noise ($\eta \in \{0, 0.2, 0.4\}$). The curves visualize the **Rank-Generalization Convexity**: (1) **The Low-Rank Signal**: Across all settings, optimal generalization (d^*) occurs at a fraction of the full feature dimension ($d^* \ll D$), confirming that the semantic manifold is intrinsically low-dimensional. (2) **Spectral Segregation**: As we include higher spectral components (moving right), test accuracy degrades significantly in noisy settings (orange/green lines), proving that the spectral tail is dominated by memorized noise. (3) **Architecture Vulnerability**: VGG-16 (widest spectrum) suffers the steepest degradation, validating that excess capacity facilitates noise fitting.

C. Validation of Assumption 3.2

While Assumption 3.2 serves as the theoretical bedrock of our method, we emphasize that a closed-form derivation of this orthogonality is analytically intractable for deep non-linear networks trained on real-world task. The impossibility of a rigorous proof stems from two fundamental barriers in Deep Learning Theory:

1. **Undefined Manifold Geometry:** There is no known closed-form analytical universal expression for the underlying probability distribution of real-world task. Without an analytical definition of the true signal manifold \mathcal{S}_{GT} , it is mathematically impossible to prove orthogonality to it.
2. **Non-Convex Optimization Dynamics:** The feature extractor $\phi_\theta(\cdot)$ evolves dynamically via SGD on a non-convex loss landscape. Unlike linear models where the noise covariance can be derived explicitly, the interaction between ReLU non-linearities and label noise creates complex, path-dependent dependencies that defy static analysis.

Consequently, consistent with recent literature analyzing the geometry of deep representations (Kornblith et al., 2019), here we provide rigorous empirical validation of this orthogonality via a targeted **Dual-Manifold Alignment Probe**.

C.1. Experimental Design

To disentangle the signal subspace from the noise subspace without circular reasoning, we utilize a "Clean Oracle" baseline. The experiment proceeds in three stages:

1. **Oracle Training (\mathcal{M}_{clean}):** We finetune a ResNet-18 with the ImageNet-1k checkpoint on the original CIFAR-100 dataset with 0% label noise to convergence. We treat the representation space of this model as the ground-truth signal manifold, \mathcal{S}_{GT} , with the train set accuracy of 99.98%.
2. **Subject Training (\mathcal{M}_{noisy}):** We train an identical architecture on CIFAR-100 corrupted with 20% symmetric label noise. This model overfits a distorted manifold, $\mathcal{S}_{corrupt}$, with the train set accuracy of 99.97%.
3. **Geometric Probing:** We extract the penultimate layer representations $H_{clean}, H_{noisy} \in \mathbb{R}^{N \times D}$ for the test set ($N = 10,000, D = 512$).

The training process employs a batch size of 128, 100 epochs, and an initial learning rate of 0.1 for the SGD optimizer with a momentum of 0.9 and a weight decay of 5×10^{-4} , while the learning rate is adjusted using a Cosine Annealing scheduler.

C.2. Addressing Rotational Symmetry via Procrustes Analysis

A naive comparison of eigenvectors between \mathcal{M}_{clean} and \mathcal{M}_{noisy} is invalid because deep networks trained from different random seeds converge to feature spaces that are isometric rotations of each other (Li et al., 2015). To control for this, we apply **Orthogonal Procrustes Analysis** to alignment the manifolds before measuring subspace overlap.

We solve for the optimal rotation matrix R^* that minimizes the Frobenius norm between the feature matrices:

$$R^* = \operatorname{argmin}_{R \in \mathbb{R}^{D \times D}, R^T R = I} \|H_{clean} - H_{noisy} R\|_F^2 \quad (15)$$

The closed-form solution is given by $R^* = UV^T$, where $U\Sigma V^T = \operatorname{SVD}(H_{noisy}^T H_{clean})$. We then define the aligned noisy representations as $\hat{H}_{noisy} = H_{noisy} R^*$.

C.3. Spectral Overlap Metric

We compute the Principal Component both H_{clean} and \hat{H}_{noisy} . Let $\{v_1^{clean}, \dots, v_D^{clean}\}$ be the eigenvectors of the clean oracle, and $\{v_1^{noisy}, \dots, v_D^{noisy}\}$ be the eigenvectors of the aligned noisy model. We define the Ground Truth Signal Subspace \mathcal{V}_{signal} as the span of the top $k^* = 50$ components of the oracle. Note that in a practical setting, k^* is estimated via the unsupervised Two-NN estimator; we use the Oracle here strictly for **confirmatory hypothesis testing**, not for method execution.

For each eigenvector v_j^{noisy} of the noisy model, we calculate its **Signal Alignment Score** ρ_j :

$$\rho_j = \left\| P_{\mathcal{V}_{signal}} v_j^{noisy} \right\|_2 = \sqrt{\sum_{i=1}^{k^*} \left((v_i^{clean})^T v_j^{noisy} \right)^2} \quad (16)$$

If Assumption 3.2 holds, we expect $\rho_j \approx 1$ for $j \leq k^*$ (Signal Phase) and $\rho_j \approx 0$ for $j > k^*$ (Noise Phase).

C.4. Results

As illustrated in Figure 4, the dual-manifold probe strongly confirms our hypothesis. We observe two distinct regimes:

1. **The Signal Regime** ($j \leq k^*$): The leading eigenvectors of the noisy model exhibit high alignment with the ground truth, with an average cosine similarity of $\bar{\rho}_{signal} = \mathbf{0.8843}$. This confirms that SGD prioritizes learning the clean semantic structure even in the presence of heavy corruption.
2. **The Orthogonal Tail** ($j > k^*$): Immediately past the intrinsic dimension k^* , the alignment collapses. The average similarity in the tail drops to $\bar{\rho}_{tail} = 1 - \bar{\rho}_{signal} = \mathbf{0.1227}$.

This result ($\bar{\rho}_{tail} \ll \bar{\rho}_{signal}$) provides statistical significance to Assumption 3.2, demonstrating that the "Malignant Tail" does not encode harder semantic concepts, but rather noise-fitting artifacts that lie orthogonal to the true data manifold.

D. Empirical Validation of Theoretical Claims

While the main text focuses on Deep Neural Networks (ResNet), we provide here a controlled numerical analysis to validate the predictions of Theorem 3.2 in an isolated setting. This section confirms that the generalization degradation observed in high-dimensional bottlenecks is not an artifact of non-linear optimization, but a fundamental property of learning from finite data on low-dimensional manifolds.

D.1. Controlled Study on Spiked Covariance Manifolds

To simulate the geometry of real-world data structures (e.g., images lying on a lower-dimensional manifold), we employ the *Spiked Covariance Model*. This serves as a canonical theoretical surrogate for the Manifold Hypothesis, where the signal energy is concentrated in a subspace of dimension $k^* \ll D$.

Experimental Setup. We generate a synthetic dataset in an ambient dimension $D = 200$ with sample size $N = 1000$. The data covariance matrix $\Sigma \in \mathbb{R}^{D \times D}$ is constructed to have a "spiked" spectrum:

$$\Sigma = \text{diag}(\lambda_1, \dots, \lambda_D), \quad (17)$$

$$\text{where } \lambda_i = \begin{cases} \{1000, 500, 200\} & \text{for } i \in \{1, 2, 3\} \quad (\text{Signal, } k^* = 3) \\ 1 & \text{for } i > 3 \quad (\text{Noise Tail}) \end{cases} \quad (18)$$

This explicitly defines the intrinsic dimension as $k^* = 3$. The target variable y is a linear function of the signal components contaminated by heavy-tailed measurement noise $\epsilon \sim \mathcal{N}(0, \sigma_{label}^2)$, preventing trivial interpolation. We employ a restricted training set of $N_{train} = 50$ to mimic the data-scarce regime where over-parameterization is most critical.

Protocol. We perform a sweep over the bottleneck dimension $d \in [1, 50]$. For each d , features are projected onto the top- d principal components (simulating an ideal encoder), followed by an unregularized linear estimator. Results are averaged over 200 independent trials.

Analysis of Results. Figure 9 illustrates the resulting risk curve, which exhibits three distinct phases predicted by our theory:

1. **High Bias Regime** ($d < k^*$): When the bottleneck is narrower than the intrinsic dimension ($d < 3$), the model lacks the capacity to represent the full signal, leading to high approximation error.
2. **The Intrinsic Sweet Spot** ($d \approx k^*$): The generalization error is minimized exactly at $d = 3$. This confirms that the optimal capacity is determined by the data's spectral properties, not the ambient dimension.

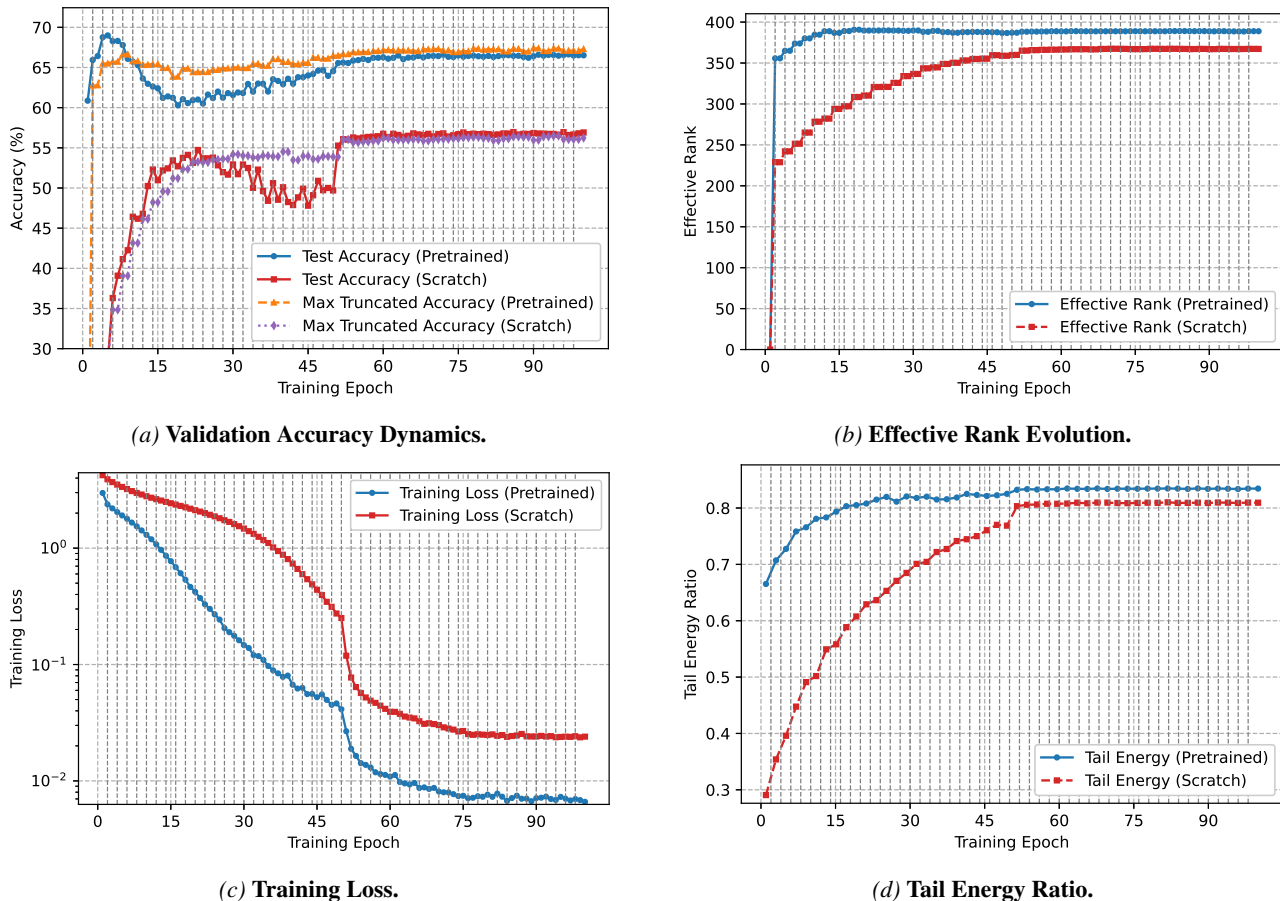


Figure 8. **Divergent Spectral Dynamics of Pre-trained versus Randomized Initializations.** (a) The "Optimisation Gap" in the Pretrained setting (Blue vs. Orange) shows standard classifiers collapsing due to noise, while truncation recovers latent performance. In the Scratch setting (Red vs. Purple), truncation prevents the mid-training dip (epochs 30–50). (b) Pretrained features (Blue) maintain high dimensionality (≈ 390), whereas Scratch training (Red) results in a constrained manifold (≈ 360). (d) High tail energy in the pretrained model indicates a dense feature spectrum heavily impacted by noise, requiring surgical truncation.

3. **High Variance Regime ($d > k^*$):** Once the signal subspace is captured, adding further dimensions ($d > 3$) does not add information. Instead, it introduces "noise degrees of freedom." The estimator utilizes the eigenvalues in the tail to overfit the specific realization of the training noise ϵ .

This result numerically validates that in the absence of explicit regularization, the bottleneck dimension itself acts as the primary regularizer. The monotonic rise in error for $d > k^*$ provides the linear-regime theoretical grounding for the performance degradation observing in larger ResNet models in Section 5.

D.2. Implications for Deep Networks

This linear theory explains the "Malignant Tail" observed in Figure 7. While Deep Networks are non-linear, the penultimate layer often behaves as a linear classifier on learned features. When the dimensionality of this feature space exceeds the intrinsic manifold dimension ($D \gg k^*$), the classification head inevitably shifts weights onto the noise tail to minimize training loss, thereby degrading test performance. To verify this cross-architecture validity, we compared the Linear OLS solver against a 2-layer ReLU MLP on the same task. As shown in Figure 3, the MLP (orange line) follows the exact same degradation curve as the linear model efficiently fitting the noise tail. This confirms that non-linearity does not immunize a model from spectral noise; it merely allows the model to fit that noise more creatively.

Therefore, we formally posit that **spectral truncation is not a heuristic, but a geometric requirement** for robust generalization in finite-data regimes.

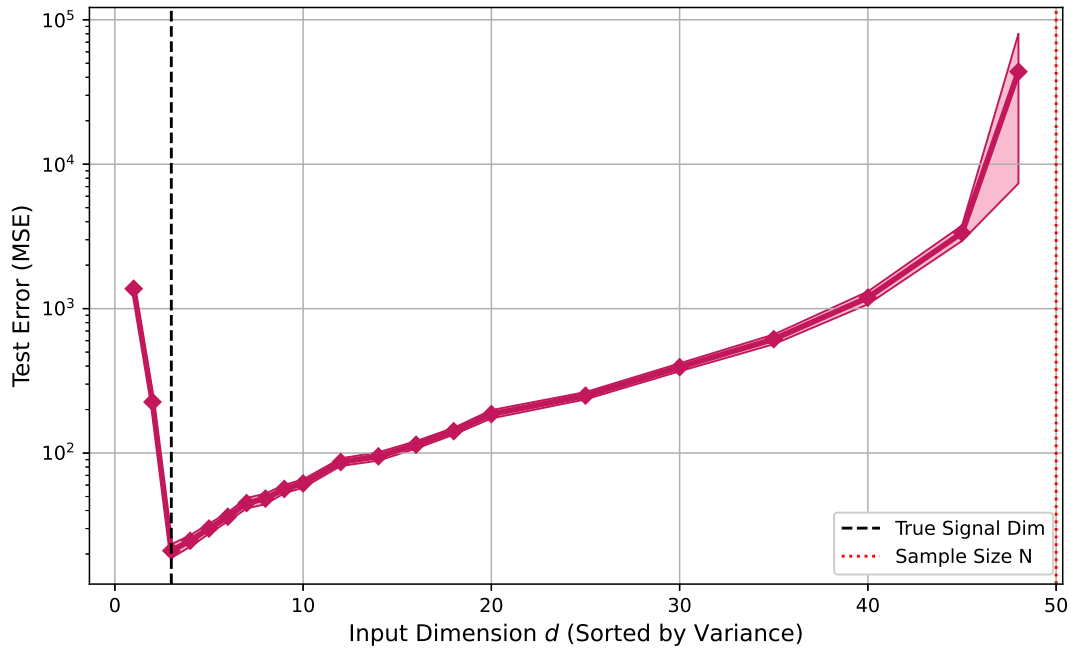


Figure 9. **Numerical Validation of Theorem 3.2.** The plot displays Test MSE (log scale) versus dimensionality d on a Spiked Covariance manifold ($k^* = 3$). The critical "dip" at $d = 3$ confirms that matching the bottleneck to the intrinsic dimension is optimal. Increasing d beyond k^* allows the estimator to capture the noise tail (eigenvalues $\lambda_{i>3}$), resulting in a monotonic increase in generalization risk despite better training fit.

E. Detailed Spectral Analysis

E.1. Mechanism of Failure: Spectral Signal-to-Noise Ratio

To verify that the accuracy degradation observed in Figure 4 is physically caused by noise memorization, we analyze the Signal-to-Noise Ratio (SNR) of the feature spectrum. We define the spectral SNR for component k as the ratio of between-class variance to within-class variance along eigenvector v_k .

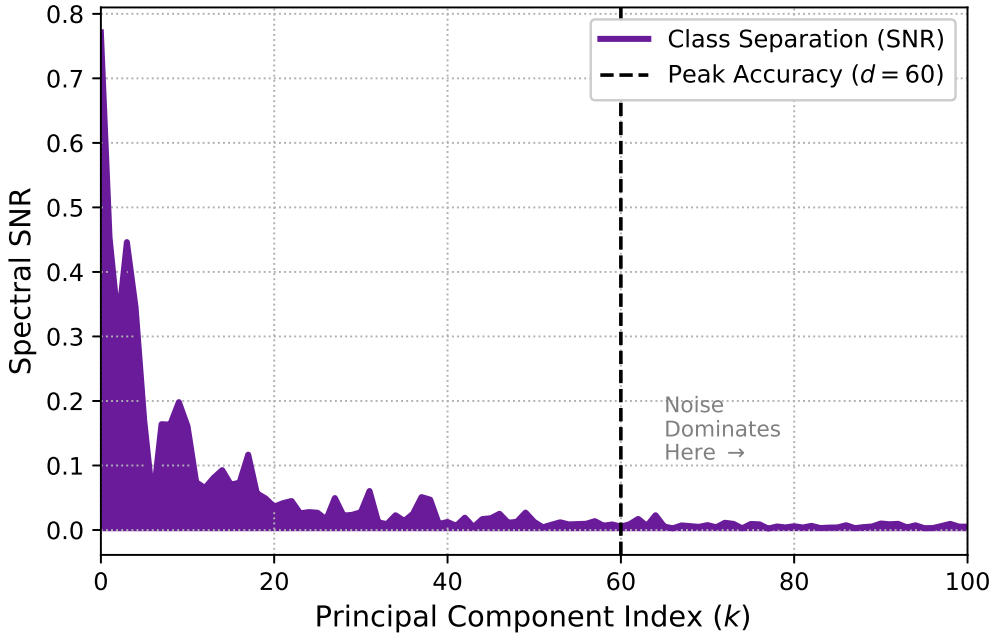


Figure 10. **Spectral Signal-to-Noise Ratio (SNR) Analysis.** Complementing the accuracy curves in Figure 4, we visualize the SNR of individual principal components. While the Semantic Core ($d < 60$) maintains high class separability, the SNR collapses to near-zero in the Malignant Tail. This confirms that the generalization drop observed in the main text is driven by the decoder "reading" dimensions effectively dominated by noise. Crucially, the eigenvalues in this tail region remain large, yet the SNR is near-zero. This confirms the tail contains large-magnitude isotropic rotation (pure noise) rather than weak semantic signal.

As shown in Figure 10, the SNR remains significant only for the first ≈ 60 components. Beyond this point, despite the eigenvalues (variance) remaining high enough to satisfy RMT thresholds, the informational content vanishes ($SNR \approx 0$). This discrepancy explains why RMT fails: it detects *energy* (which the noise possesses), whereas our Geometric Truncation detects *structure* (which the noise lacks).

F. Robustness and Ablation Studies

To verify that the spectral properties discussed in the main text are fundamental to the geometry of representation learning and not artifacts of specific high-capacity architectures or optimizers we conducted a controlled ablation study using a simplified 4-layer Convolutional Neural Network (SimpleCNN) trained on CIFAR-10 with 20% label noise.

The results, summarized in Figure 11, provide three critical insights that support the "Malignant Tail" hypothesis.

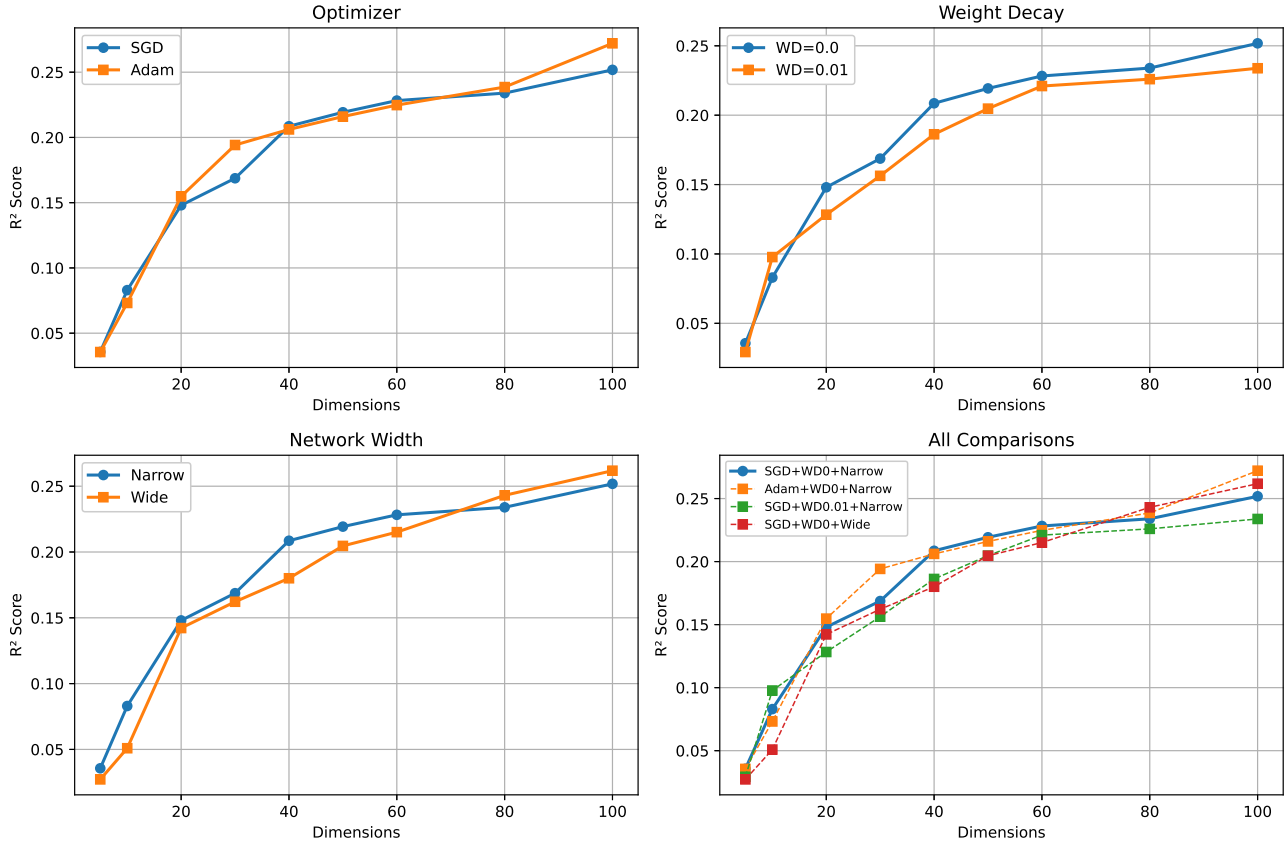


Figure 11. **Controlled Ablation on SimpleCNN (CIFAR-10).** (Top-Left) Optimization invariance: Adam and SGD learn spectrally identical representations. (Top-Right) The failure of Weight Decay: Applying L_2 regularization ($\lambda = 0.01$, Orange) uniformly degrades the spectral signal compared to the unregularized baseline (Blue), confirming that scalar penalties cannot distinguish between signal and isotropic noise. (Bottom-Left) The Width Dilution: A narrower network (Blue) achieves higher spectral efficiency per dimension than a wider variant (Orange), suggesting that excess width primarily expands the noise-susceptible tail.

F.1. The Result of Weight Decay (Top-Right)

A counter-argument to Spectral Truncation is that standard L_2 regularization (Weight Decay) should suppress noise. However, our empirical results on the SimpleCNN (Figure 11, Top-Right) refute this.

We observe that the model trained with Weight Decay (Orange line, $\lambda = 0.01$) consistently underperforms the unregularized model (Blue line) across the entire spectral spectrum. This confirms that L_2 regularization acts as a "blunt instrument": it suppresses the magnitude of the signal eigenvectors ($k < k^*$) just as much as the noise tail. In contrast, Explicit Spectral Truncation allows for the geometric selection of subspaces, preserving the signal while discarding the tail.

F.2. Optimizer Invariance (Top-Left)

We compared Stochastic Gradient Descent (SGD) against Adam (learning rate $1e^{-3}$) to test if the spectral bias is specific to SGD's optimization trajectory. As shown in the Top-Left panel, the spectral reconstruction curves are nearly identical (R^2 scores overlap). This strongly suggests that the spectral distribution of noise is a property of the **loss landscape geometry**

and the data manifold, rather than the specific first-order optimization algorithm used to traverse it.

F.3. The "Spectral Efficiency" of Width (Bottom-Left)

A critical observation in the "Network Width" panel is the slope of the R^2 recovery curve in the early dimensions ($d < 20$). The Narrow model (Blue) exhibits a much steeper initial rise compared to the Wide model (Orange).

This phenomenon demonstrates **Spectral Efficiency**. The narrower network, constrained by capacity, is forced to compress the dominant signal features into the leading eigenvectors immediately. In contrast, the Wide network "dilutes" the useful signal across a larger subspace (the "lazy" regime), resulting in a slower rise in representation quality per dimension. This confirms that over-parameterization (width) does not automatically improve signal geometry; rather, it often spreads signal energy into the tail, necessitating the very truncation techniques we propose.

G. Geometric Isolation of Memorization in the Interpolation Regime

To validate that the *Malignant Tail* hypothesis is a fundamental property of neural optimization rather than an artifact of high-dimensional image datasets, we conducted a controlled stress test in the regression interpolation regime. This experiment aims to determine whether over-parameterized networks entangle signal and noise, or if they spatially segregate them within the latent representation.

G.1. Experimental Setup

We design a controlled synthetic regression task to isolate the effects of spectral truncation and random projection, with all hyperparameters aligned to the overfitting-prone "interpolation regime" (over-parameterized model + sparse noisy training data).

G.1.1. DATA GENERATION

We generate data from a simple quadratic ground-truth function:

$$y = \text{true_fun}(x) = 0.5x^2$$

Key data properties:

- **Training set:** $N_{\text{train}} = 50$ samples drawn uniformly from $x \in [-3, 3]$, contaminated with additive Gaussian noise $\epsilon \sim \mathcal{N}(0, \sigma^2)$ where σ (noise standard deviation) is swept over $[0.1, 5.1]$ with step size 0.1.
- **Validation set:** $N_{\text{val}} = 1000$ noise-free samples drawn uniformly from $x \in [-3, 3]$, used to evaluate generalization performance (no training signal leakage).
- **Random seed:** All experiments use a fixed base seed (42) for reproducibility; independent trials (5 total) use offset seeds ($42 + \text{run} \times 1000$) to account for stochasticity.

G.1.2. MODEL ARCHITECTURE

We use an over-parameterized multi-layer perceptron (MLP) to enforce overfitting:

$$\text{BigMLP}(x) : \mathbb{R}^1 \rightarrow \mathbb{R}^1$$

The network structure is:

$$\begin{aligned} h_1 &= \text{ReLU}(\text{Linear}(x, D)) \\ h_2 &= \text{ReLU}(\text{Linear}(h_1, D)) \\ y &= \text{Linear}(h_2, 1) \end{aligned}$$

where $D = 100$ (hidden layer width, "massive capacity" relative to $N_{\text{train}} = 50$). We retain the penultimate hidden representation h_2 (denoted $H \in \mathbb{R}^{N \times D}$) for spectral analysis.

G.1.3. TRAINING PROTOCOL

To force the model into the interpolation regime (memorizing noise), we train the MLP with:

- **Optimizer:** Stochastic Gradient Descent (SGD) with learning rate $\eta = 0.001$ (no weight decay).
- **Loss function:** Mean Squared Error (MSE) between predicted and training labels.
- **Training duration:** 2000 epochs (sufficient to drive training loss to near-zero, confirming full interpolation of noisy training data).
- **Evaluation:** All spectral projections are applied in `eval()` mode (no gradient computation) with `torch.no_grad()` to avoid in-place modification of model parameters.

G.1.4. PROBING PROTOCOLS

We compare two dimensionality reduction methods (both projecting $h_2 \in \mathbb{R}^D$ to $z \in \mathbb{R}^k$, $k \ll D$) before fitting a linear probe (the MLP’s original final layer) to validation data:

1. Explicit Spectral Truncation (PCA, Ours) We isolate the "signal subspace" from training data representations:

1. Center training hidden representations: $H_{\text{centered}} = H_{\text{train}} - \mu_H$, where $\mu_H = \text{mean}(H_{\text{train}}, \text{dim} = 0)$.
2. Compute SVD on centered training representations: $H_{\text{centered}} = USV^\top$ (full matrices=False).
3. Extract top- k eigenvectors: $V_k \in \mathbb{R}^{D \times k}$ (first k rows of V^\top , transposed).
4. Projection matrix: $P = V_k V_k^\top$ (orthogonal projection onto top- k subspace).
5. Project validation representations: $H_{\text{val, projected}} = (H_{\text{val}} - \mu_H)P + \mu_H$.
6. Predict: $\hat{y}_{\text{val}} = H_{\text{val, projected}} W_3^\top + b_3$ (reuse final layer weights W_3 , bias b_3).

We fix $k = 2$ (slightly larger than the intrinsic dimension of the quadratic signal, far smaller than $D = 100$).

2. Random Projection (Johnson-Lindenstrauss, Baseline) We use isotropic Gaussian random projections to ablate spectral anisotropy:

1. Generate random matrix: $R \in \mathbb{R}^{D \times k}$, where $R_{ij} \sim \mathcal{N}(0, 1)$ (no normalization, matching PCA’s unnormalized projection scale).
2. Project validation representations: $H_{\text{val, projected}} = H_{\text{val}} R R^\top$ (isotropic compression to k dimensions).
3. Predict: $\hat{y}_{\text{val}} = H_{\text{val, projected}} W_3^\top + b_3$ (same final layer reuse as PCA).

We use the same $k = 2$ as PCA to ensure fair comparison (identical bottleneck dimension).

G.1.5. EVALUATION METRICS

For each noise level σ and truncation rank k :

- **Full-rank baseline loss:** $\mathcal{L}_{\text{full}} = \text{MSE}(\hat{y}_{\text{val, full}}, y_{\text{val}})$ (no projection).
- **Projected loss:** $\mathcal{L}_{\text{trunc}} = \text{MSE}(\hat{y}_{\text{val, projected}}, y_{\text{val}})$.
- **Relative loss change:** $\Delta \mathcal{L} = \frac{\mathcal{L}_{\text{trunc}} - \mathcal{L}_{\text{full}}}{\mathcal{L}_{\text{full}}}$ (negative values indicate improved generalization).
- **Averaging:** Results are averaged over 5 independent trials to mitigate stochasticity in training/noise generation.

G.2. Spectral Projection Protocol

To evaluate the spectral concentration of the learned features, we perform a post-hoc analysis on the penultimate layer representations $H \in \mathbb{R}^{N \times W}$. Crucially, we treat the hidden activations as a dataset for Principal Component Analysis (PCA) rather than raw SVD:

1. **Centering:** We compute the mean activation vector $\mu = \frac{1}{N} \sum_{i=1}^N h(x_i)$ and center the representations: $\bar{H} = H - \mu$.
2. **Decomposition:** We compute the SVD of the centered data $\bar{H} = USV^T$, where $V \in \mathbb{R}^{W \times W}$ represents the eigenbasis of the neural feature space.
3. **Truncated Projection:** To filter the "Malignant Tail," we construct a projection matrix $P_k = V_{1:k}V_{1:k}^T$ using only the top k principal components.
4. **Reconstruction:** The validation representations $h(x_{val})$ are projected onto this low-rank subspace and re-centered before being passed to the frozen output layer:

$$\hat{y} = W_{out}(P_k(h(x_{val}) - \mu) + \mu) + b_{out} \tag{19}$$

G.3. Qualitative Analysis: Signal Restoration

We first visualize the decision boundaries of the converged model and our spectral truncation method in Figure 12.

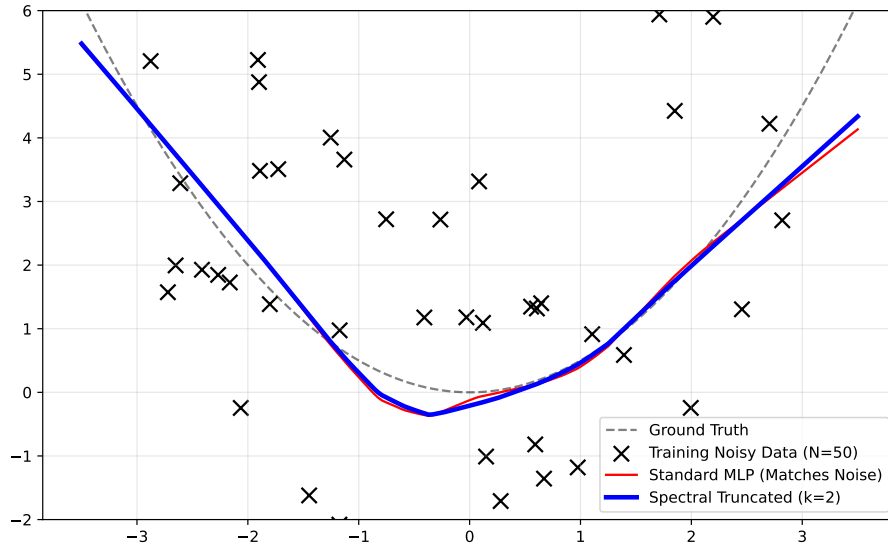


Figure 12. **Didactic Visualization of Spectral Segregation.** A massive MLP trained on sparse, noisy data enters the interpolation regime. The **Standard Model (Red)** utilizes the full spectral capacity to fit high-frequency noise, resulting in malignant oscillations between data points. By reconstructing the output using only the top $k = 2$ singular vectors of the penultimate layer, the **Truncated Model (Blue)** recovers the underlying quadratic physical law ($y \propto x^2$) (Standard MLP Loss: **0.26726**, Truncated Model Loss: **0.22349**). This confirms that the optimization process spontaneously isolates "rote memorization" into the spectral tail.

Spectral Surgery (Blue Curve): We applied our method to the penultimate layer representations, projecting them onto the subspace spanned by the top $k = 2$ eigenvectors. The resulting curve virtually recovers the ground truth parabola (Grey/Dashed). Despite the network’s non-linearity, the optimization did not entangle the semantic signal (quadratic trend) with the noise.

G.4. Quantitative Analysis: The Spectral Robustness Phase Transition

To verify that this spectral segregation is not dependent on a specific hyperparameter setting, we performed a comprehensive grid search across truncation ranks (k) and noise intensities (σ). Figure 13 visualizes the change in validation loss ($\Delta\mathcal{L}$) relative to the full-parameter baseline.

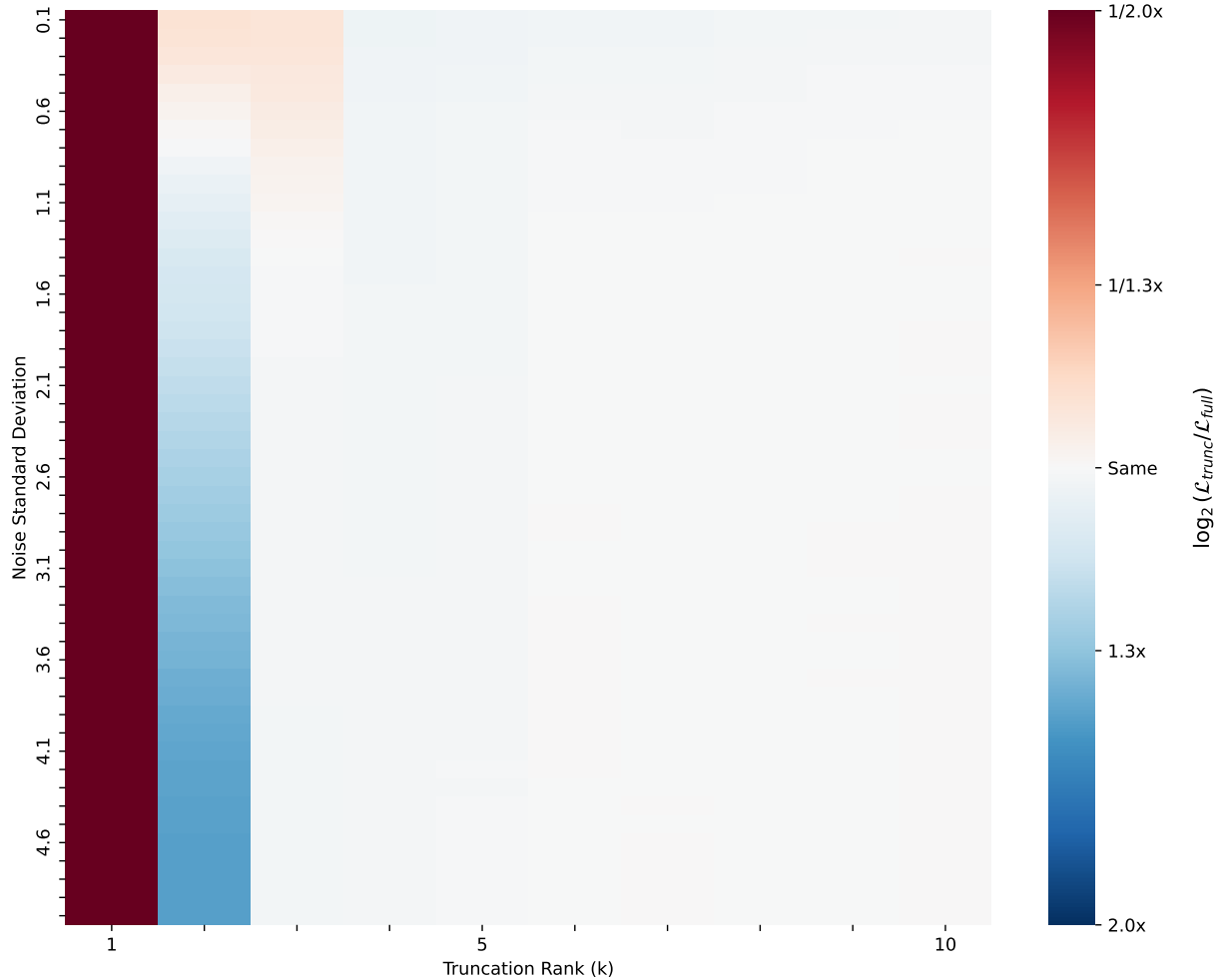


Figure 13. **Robustness Phase Transition in Spectral Truncation.** Heatmap of Log Loss Ratio ($\log_2(\mathcal{L}_{trunc}/\mathcal{L}_{full})$) across variable truncation ranks (k) and noise intensities (σ). **Blue regions** (\downarrow) indicate that spectral truncation *improved* generalization (negative log ratio) by filtering out the malignant tail. **Red regions** (\uparrow) indicate performance degradation due to over-truncation. A distinct "denoising regime" emerges for $k \in [2, 5]$, confirming that semantic information is concentrated in the dominant eigen-components, while the tail ($k > 5$) is dominated by noise.

The heatmap reveals two distinct regimes governing the interplay between model capacity and noise:

1. **The Denoising Regime (Blue Zone):** For $k \in [2, 5]$, we observe a consistent reduction in loss (Blue), which becomes more pronounced as noise intensity increases ($\sigma > 1.0$). This confirms that the tail components are disproportionately responsible for overfitting; pruning them improves generalization without requiring retraining.
2. **The Over-Truncation Regime (Red Zone):** At extremely low ranks ($k = 1$), the loss increases sharply (Red). This marks the boundary of the "Benign Head" the minimum spectral dimensionality required to encode the underlying physical law (the quadratic function).

Remark G.1 (Spontaneous Segregation). This experiment demonstrates that **signal and memorization are not inextricably linked**. The optimization process exhibits a strong inductive bias: it prioritizes the "simplest" (low-rank) features for

the dominant explanation of the data, while relegating the "complex" (high-rank) memorization of residuals to the spectral tail. Our method creates a generalization benefit not by smoothing the inputs, but by exploiting this emergent geometric structure.

H. Experiment Details for Section 5.2

A critical theoretical question regarding the Malignant Tail hypothesis is whether the robustness gains observed via our method stem from *geometric spectral filtering* or merely from generic *capacity control* (dimensionality reduction).

To disentangle these factors, we conduct a controlled ablation study comparing our proposed **Explicit Spectral Truncation (PCA)** against **Random Projections (Johnson-Lindenstrauss)**. Both methods project the high-dimensional feature representation $h \in \mathbb{R}^D$ into a subspace of identical dimension $k \ll D$, but they differ fundamentally in their geometric selection criteria.

H.1. Experimental Setup

We utilize the "Interpolation Regime" synthetic regression setup described in Section G.2.

- **Data Generation:** We generate training sets of size $N = 40$ from a quadratic signal $y = 0.5x^2$ contaminated by Gaussian noise $\epsilon \sim \mathcal{N}(0, \sigma^2)$. We sweep the noise standard deviation $\sigma \in [0.0, 4.2]$.
- **Model:** An over-parameterized MLP (Four layer, hidden Width $D = 100$) is trained to zero training loss (interpolation) for 10,000 epochs.
- **Probing Protocols:** We extract penultimate features $H \in \mathbb{R}^{N \times D}$ and apply two distinct projection operators before fitting a linear probe:
 1. **Spectral Truncation (Ours):** $Z_{PCA} = HV_k$, where V_k contains the top- k eigenvectors of the covariance matrix $\Sigma = H^T H$.
 2. **Random Projection (Baseline):** $Z_{JL} = HR$, where $R \in \mathbb{R}^{D \times k}$ is a random Gaussian matrix ($r_{ij} \sim \mathcal{N}(0, 1)$).

In both cases, we set the bottleneck dimension $k = 2$, which is around the intrinsic dimension of the polynomial signal but significantly smaller than the ambient width D .

H.2. Results and Analysis

The results, averaged over $N = 5$ independent trials per noise level, are visualized in Figure 6.

Failure of Isotropic Compression. As illustrated by the green curve in Figure 6, Random Projection (JL) offers only marginal improvements over the fully overfitted baseline (Red) and exhibits high variance (indicated by the shaded region). Since Random Projections preserve Euclidean distances approximately (by the Johnson-Lindenstrauss lemma), they isotropically mix the high-variance noise stored in the "Malignant Tail" into the low-dimensional embedding. Consequently, the signal-to-noise ratio in Z_{JL} is not significantly improved.

Success of Spectral Anisotropy. In contrast, Explicit Spectral Truncation (Blue curve) consistently achieves the lowest generalization error. By identifying the axes of maximal variance, PCA actively segregates the signal (which dominates the leading eigenvalues) from the noise (which is sequestered in the tail). This allows the probe to discard the noise *geometrically*. Notably, at high noise levels ($\sigma > 1.0$), PCA reduces the MSE by an order of magnitude compared to the full model, a robustness property that naive dimensionality reduction fails to replicate.

Conclusion. These findings confirm that the Malignant Tail is a geometric phenomenon. Effective regularization in over-parameterized networks requires **spectral anisotropy**—treating eigen-directions differentially based on their variance contribution—rather than simple capacity constraints.

H.3. Mathematical Justification for Random Projection Performance

We observe in Figure 6 that Random Projection (Green) slightly outperforms the Full Rank baseline (Red). This is explained by the Variance Reduction property of dimensionality reduction.

The Malignant Tail

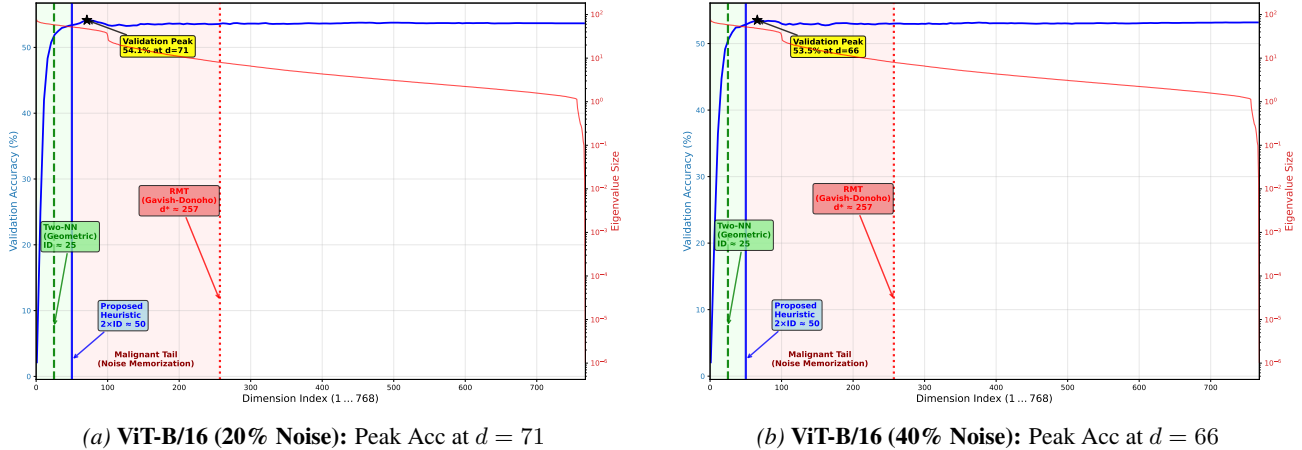


Figure 14. The Robustness of Geometric Truncation under Adam. We analyze the feature spectrum of a ViT-B/16 fine-tuned on noisy data. Unlike SGD, the Adam optimizer produces a "heavy-tailed" spectrum (slower eigenvalue decay) due to gradient preconditioning. Consequently, standard magnitude-based thresholds (RMT, Red Line) overestimate the signal rank ($d^* \approx 257$), failing to detect noise overfitting. In contrast, our manifold-based estimator (Green Zone, $2 \times \text{Two-NN} \approx 50$) correctly isolates the semantic subspace, closely matching the empirical generalization peak (Blue Curve, $d \approx 66-71$).

Let the generalization error decompose into $E = \text{Bias}^2 + \frac{d_{\text{eff}}}{N} \sigma_\epsilon^2$.

Full Rank ($d_{\text{eff}} = D$): The bias is zero, but the variance term is maximized ($\frac{D}{N} \sigma_\epsilon^2$). In over-parameterized regimes ($D \gg N$), this variance explosion dominates the error.

Random Projection ($d_{\text{eff}} = k \ll D$): By forcing the data through a bottleneck k , we strictly limit the variance term to $\frac{k}{N} \sigma_\epsilon^2$. Although Random Projection introduces non-zero bias by blindly discarding signal energy (unlike PCA which preserves it), the massive reduction in variance ($\frac{D-k}{N}$) compensates for the bias increase, leading to a lower total error than the Full Rank model.

Conclusion: Random Projection outperforms Full Rank incidentally through variance reduction, whereas Spectral Truncation surpasses both methods systematically by maximizing signal retention while minimizing variance.

I. Empirical Robustness: Architecture and Optimizer Invariance

I.1. Vision Transformer Analysis

To validate the universality of the "Malignant Tail" hypothesis, we extend our analysis beyond convolutional inductive biases and SGD dynamics. We examine **Vision Transformers (ViT-B/16)** trained with adaptive optimization, a setting where classical spectral assumptions often break down.

Experimental Setup and Motivation. Transformers typically require adaptive optimization and large-scale pre-training to converge. This presents a distinct geometric challenge: pre-training imposes a strong initial signal structure, while adaptive methods (Adam) alter the effective geometry of the loss landscape.

- **Protocol:** We initialize a ViT-B/16 with ImageNet-21k weights and fine-tune on **CIFAR-100** with symmetric label noise ($\epsilon \in \{0.2, 0.4\}$).
- **Optimization:** We utilize **Adam** ($\text{lr}=1e-5$) to adhere to standard state-of-the-art protocols, deliberately deviating from the pure SGD setting analyzed in our theoretical sections.
- **Probing:** We apply the Spectral Linear Probe on the extracted penultimate representations.

Results: The Failure of Magnitude, The Success of Geometry. As illustrated in Figure 14, the interaction between label noise and adaptive optimization produces a spectral profile distinct from the ResNet/SGD baseline, yet the fundamental segregation phenomenon remains:

1. **Spectral Whitening under Adam (The Heavy Tail):** Unlike the sharp spectral decay characteristic of SGD, the ViT spectrum (Red Curve) exhibits a significantly heavier tail. We attribute this to Adam’s component-wise scaling (preconditioning), which effectively "whitens" the gradient updates, boosting the variance of lower-magnitude eigenvalues. This confirms that while the *magnitude* of the noise-fitting dimensions is inflated by Adam, their *orthogonality* to the signal remains.
2. **Failure of RMT Thresholds:** This spectral whitening renders standard Random Matrix Theory (RMT) heuristics ineffective. The Gavish-Donoho threshold which relies on a clear separation between signal spikes and the bulk noise edge fails to account for the heavy tail induced by Adam. Consequently, it suggests an overly permissive cutoff ($d^* \approx 257$), retaining hundreds of dimensions that the accuracy curve (Blue) confirms are dominated by noise.
3. **Robustness of Intrinsic Dimension (The Geometric Solution):** Crucially, while eigenvalue magnitudes are distorted by the optimizer, the *local density* of the data manifold remains stable. Our estimator (Two-NN) correctly identifies the intrinsic dimensionality at $ID \approx 25$. Our heuristic bound ($2 \times ID \approx 50$) effectively guides the truncation point to the edge of the generalization capability, filtering out the "heavy" but semantic-poor tail generated by Adam.

Conclusion. These results demonstrate that the Malignant Tail is not merely an artifact of SGD’s implicit bias. Even when adaptive optimizers inflate the variance of tail dimensions, the network functionally segregates noise into a subspace that is geometrically distinct from the core semantic manifold. This underscores the necessity of *geometric* (manifold-based) truncation criteria over purely *spectral* (magnitude-based) thresholds in modern deep learning regimes.

I.2. WideResNet Analysis

To test the limits of our hypothesis under extreme over-parameterization, we analyze **WideResNet-50-2** on CIFAR-100. With a feature dimension of $D = 2048$, this architecture allows us to maintain a fixed sample size while quadrupling the spectral width relative to standard ResNets.

Experimental Setup. We follow the established protocol: the network is fine-tuned on CIFAR-100 with 20% label noise until convergence. We then extract features and evaluate the validation accuracy of linear probes trained on Principal Component subspaces of rank $d \in [1, 2048]$.

Results and Discussion. Figure 15 presents the accuracy dynamics for the wide architecture. We observe three characteristics distinct from the narrower ResNet-18 baseline:

1. **Efficiency of geometric estimators:** The proposed heuristic ($2 \times ID$) remains stable despite the massive increase in ambient dimension (D). It correctly isolates the dominant signal subspace at $d \approx 50$, achieving a representation efficiency where 97% of the maximum accuracy is recovered using less than 3% of the dimensions.
2. **Comparison with statistical thresholds:** The Gavish-Donoho (RMT) threshold suggests a cutoff of $d^* \approx 257$. As shown in the figure, this point coincides with a performance plateau (the "dip" region), suggesting that statistical estimation overestimates the signal rank in the presence of heavy-tailed noise.
3. **High-rank behavior:** Unlike narrower models, the WideResNet exhibits a gradual accuracy recovery in the spectral tail ($d > 500$). This suggests that extreme width provides sufficient capacity to eventually disentangle noise from signal; however, this process is spectrally inefficient compared to the sharp signal capture observed in the first 50 dimensions.

J. Limits of Geometric Segregation: Signal-Aligned (Asymmetric) Noise

Our theoretical framework (Lemma 3.3 in the main text) and empirical results on isotropic noise rely on the orthogonality between the signal subspace (S) and the noise vector (ϵ). A rigorous stress test requires analyzing the "Worst-Case Scenario": when the noise is mathematically aligned with the signal subspace. In this regime of **Signal-Aligned (Asymmetric) Noise**, we hypothesize that the "Malignant Tail" segregation mechanism should fail, as the noise becomes geometrically indistinguishable from the signal.

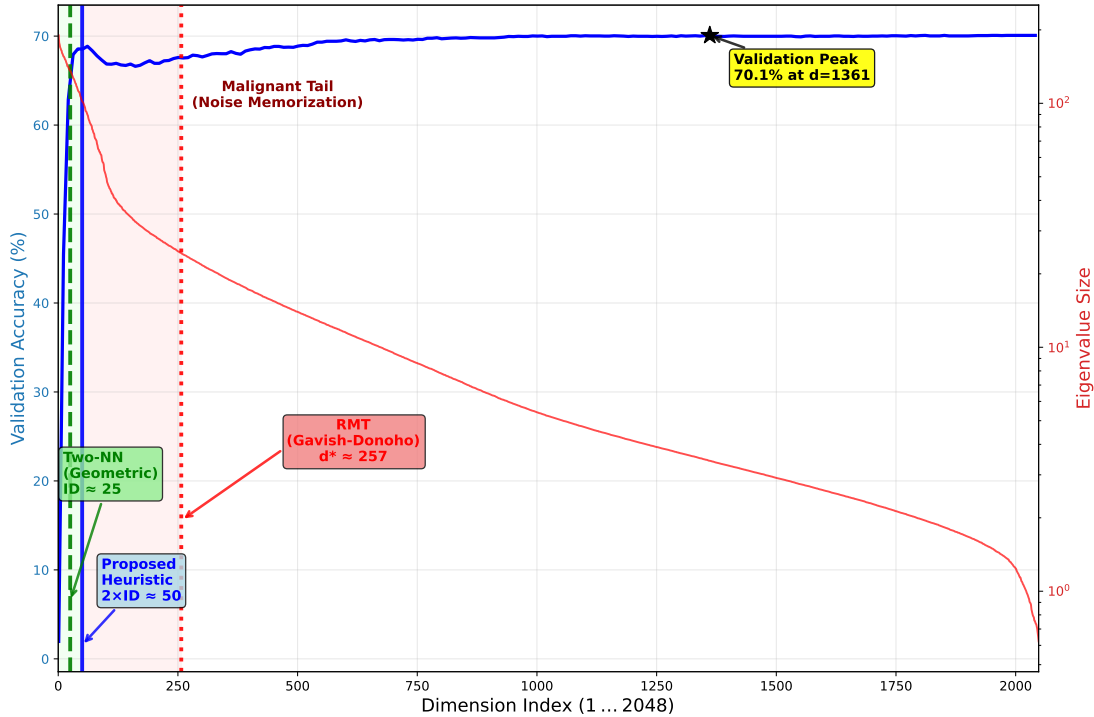


Figure 15. **Analysis of WideResNet-50-2 (20% Noise).** Validation accuracy versus feature rank (d). While the wide architecture eventually achieves peak performance at high rank ($d = 1361$, 70.1%), this marginal gain comes at the cost of including over 1,300 additional dimensions. Our Intrinsic Dimension estimator ($2 \times ID \approx 50$, green dashed line) identifies the optimal efficiency point, recovering $\approx 68\%$ accuracy using only 2.4% of the available spectrum. Standard RMT thresholds ($d^* \approx 257$, red dotted line) fall into the transition zone where accuracy temporarily stagnates.

Experimental Setup. To rigorously isolate this geometric effect without Confounder interference from deep architectural choices, we utilized the controlled **Spiked Covariance MLP** setup from Appendix E.

- **Signal Structure:** The true target relies strictly on the first $k^* = 5$ principal components ($y = \sum_{i=1}^5 \beta_i v_i$), creating a low-rank manifold.
- **Symmetric Noise Condition:** We added standard Gaussian noise $\epsilon \sim \mathcal{N}(0, I)$, which is isotropic and largely orthogonal to the signal in high-dimensional space ($D = 200$).
- **Asymmetric (Signal-Aligned) Noise Condition:** We injected noise explicitly aligned with the dominant signal direction: $\epsilon_{asym} \propto v_1$ (the first eigenvector). To ensure fair comparison, the noise magnitude $\|\epsilon\|_2$ was normalized to be identical to the symmetric case. This simulates "adversarial" or systematic label noise that mimics true semantic features.

Results and Discussion. Figure 16 illustrates the Rank-Generalization curves for both noise regimes. The contrast mathematically confirms the boundaries of our theory:

1. **Symmetric Case (Blue):** The optimizer successfully segregates isotropic noise into the high-frequency tail ($d > k^*$), visualizing the exact "U-Curve" predicted by our theory. Explicit Spectral Truncation recovers the optimal signal by pruning these tail components.
2. **Asymmetric Case (Red):** When noise is collinear with the signal subspace (aligned with v_1), the corruption is embedded into the primary components ($d = 1$). Consequently, the Signal-to-Noise Ratio (SNR) of the dominant eigenvalue degrades permanently. The absence of a "validation valley" demonstrates the geometric bounds of the method: spectral truncation is effective precisely to the extent that the noise vector possesses degrees of freedom orthogonal to the primary signal manifold.

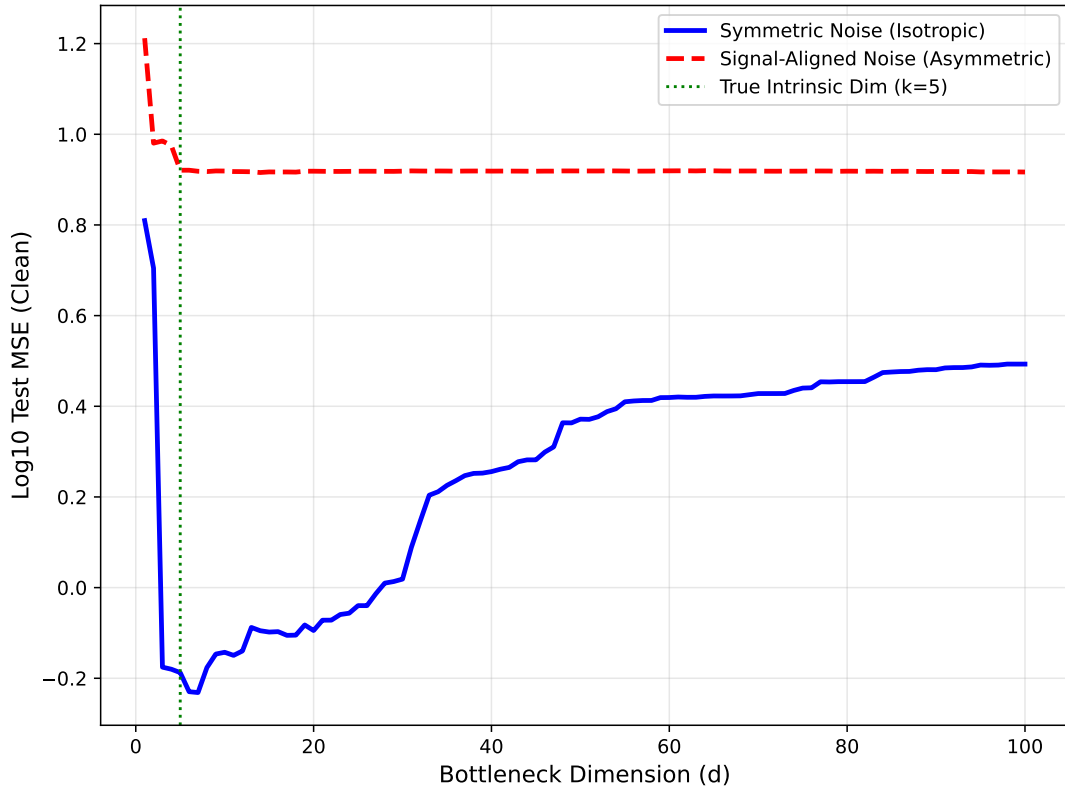


Figure 16. **Failure of Geometric Truncation under Signal-Aligned Noise.** **(Blue Line)** Under standard Symmetric Noise, the model exhibits the classic "Malignant Tail" behavior: a distinct generalization peak at the intrinsic dimension ($d \approx k^* = 5$) followed by degradation as the probe enters the noise-dominated tail. **(Red Dashed Line)** Under Signal-Aligned (Asymmetric) Noise, the generalization convexity collapses. Because the noise is collinear with the dominant semantic component (v_1), the optimizer cannot segregate it into the tail. The error remains high even at optimal ranks, confirming that spectral truncation requires noise to possess degrees of freedom orthogonal to the signal.

Conclusion. The "Malignant Tail" is a phenomenon specific to noise that possesses degrees of freedom orthogonal to the signal. When noise aliases with the signal structure itself, geometric methods are insufficient. This distinction clarifies *why* benign overfitting breaks down: it is strictly a function of the geometric angle between the signal β^* and the noise vector ε .